Accelerated pseudo-transient method for elastic, viscoelastic, and coupled hydro-mechanical problems with applications

Yury Alkhimenkov[1] and Yury Podladchikov[2]

[1]Department of Civil and Environmental Engineering, Massachusetts Institute of Technology, Cambridge, MA 02139, USA
[2]Institute of Earth Sciences, University of Lausanne, Switzerland

Correspondence: Yury Alkhimenkov (yalkhime@mit.edu)

Abstract. The Accelerated Pseudo-Transient (APT) method is a matrix-free approach used to solve partial differential equations (PDEs), characterized by its reliance on local operations, which makes it highly suitable for parallelization. With the advent of the memory-wall phenomenon around 2005, where memory access speed overtook floating-point operations as the bottleneck in high-performance computing, the APT method has gained prominence as a powerful tool for tackling various PDEs in geosciences. Recent advancements have demonstrated the APT method's computational efficiency, particularly when applied to quasi-static nonlinear problems using Graphical Processing Units (GPUs). This ~~manuscript~~ study presents a comprehensive analysis of the APT method, focusing on its application to quasi-static elastic, viscoelastic, and coupled hydro-mechanical problems, specifically those governed by quasi-static Biot's poroelastic equations, across 1D, 2D, and 3D domains. We systematically investigate the optimal numerical parameters required to achieve rapid convergence, offering valuable insights into the method's applicability and efficiency for a range of physical models. Our findings are validated against analytical solutions, underscoring the robustness and accuracy of the APT method in both homogeneous and heterogeneous media. We explore the influence of boundary conditions, non-linearities, and coupling on the optimal convergence parameters, highlighting the method's adaptability in addressing complex and realistic scenarios. To demonstrate the flexibility of the APT method, we apply it to the nonlinear mechanical problem of strain localization using a poro-elasto-viscoplastic rheological model, achieving extremely high resolutions - $10,000^2$ ~~voxels~~ in 2D and 512^3 ~~voxels~~ in 3D - that, to our knowledge, have not been previously explored for such models. Our study contributes significantly to the field by providing a robust framework for the effective implementation of the APT method in solving challenging geophysical problems. Importantly, the results presented in this paper are fully reproducible, with Matlab, symbolic Maple scripts, and CUDA C codes made available in a permanent repository.

1 Introduction

The Accelerated Pseudo-Transient (APT) method represents a powerful tool in computational science, combining efficiency, scalability, ease of implementation, and a strong theoretical foundation rooted in wave physics. The main idea of the APT method is that instead of solving the original partial differential equation (PDE), a modified PDE with added inertial terms and

attenuation is solved in iterative fashion until the inertial terms vanish. In other words, the solution of the original PDE is an attractor of the transient PDE with inertia.

The ~~APT method is an efficient iterative approach for solving PDEs without relying on matrix storage~~Accelerated Pseudo-Transient (APT) method is designed to iteratively solve a modified version of the original partial differential equation (PDE) by introducing inertial and relaxation terms. This modified PDE is repeatedly solved until the added pseudo-physical terms vanish, providing an accurate approximation of the solution to the original equation. The APT method becomes increasingly efficient when implemented with exclusively spatially local operations, eliminating the need to access global storage for evolving fields. Unlike the conjugate gradient method, which requires two global scalar products per iteration, the APT method advances without global memory operations, enhancing computational performance by utilizing fast cache memory. This method is versatile, applicable to both linear and nonlinear equations, and distinguishes itself with several key attributes. (i) APT is a matrix-free method, enabling the solution of large-scale 3D problems without the overhead of matrix storage. (ii) leveraging only local operations, APT naturally lends itself to parallelization, making it well-suited for modern computing architectures. (iii) its structure facilitates efficient implementation on Graphical Processing Units (GPUs), capitalizing on their ability to handle parallel tasks ~~effectively~~efficiently. (iv), APT method aligns closely with the physics of wave phenomena, offering a robust theoretical framework for rigorous understanding and application.

One of the first pseudo-transient (PT) iterative methods to solve elliptic PDEs was presented by Richardson (1911). ~~Probably one of the first iterative methods that features second-order iterations and can be called as APT~~ An improved PT method for elliptic problems, which can be referred to as the Accelerated Pseudo-Transient (APT) method, was proposed in the 1950s by ~~Frankel (1950); Riley (1954) for solving elliptic equations (see also Young (1972))~~Frankel (1950) and further investigated by Riley (1954) and Young (1972). The pseudo-transient method is also known as a dynamic-relaxation (DR) method that was used by Otter (1965); Otter et al. (1966). Interestingly, the APT method was also applied in other branches of science, e.g., in areas related to optimization problems (Polyak, 1964). In geosciences, the APT method was introduced as the Fast Lagrangian Analysis of Continua (FLAC) algorithm by Cundall (1976), it was applied to solve non-linear problems and instabilities (Poliakov et al., 1993a, 1994). The APT method was recently applied to model large 3D geophysical problems: coupled two-phase flow physics represented by solitary porosity waves (Räss et al., 2019), reaction-driven porosity waves (Omlin et al., 2017) and thermomechanical ice deformation (Räss et al., 2020). The APT method was applied to model focused fluid flow by Wang et al. (2022). Furthermore, Wang et al. (2022) investigated the physics-based principles underlying the APT method. A compaction-driven fluid flow and plasticity within porous media were investigated numerically by Alkhimenkov et al. (2024a). A numerical approach based on GPUs to model the strain localization in 2D and 3D of a (visco)-hypoelastic-perfectly plastic medium was developed by Alkhimenkov et al. (2024b).

The efficiency of the APT method strongly depends on the choice of the numerical parameters. For simple equations, such parameters can be derived analytically. This was done for elliptic equations by analyzing a damped wave equation (DWE) (Cox and Zuazua, 1994), since the solution of elliptic equations is an attractor of DWE. In optimization problems the APT method is also known as PDE acceleration framework (Calder and Yezzi, 2019; Benyamin et al., 2020). A comprehensive study that provides the optimal values of numerical parameters of the APT method for various problems is provided by Räss et al. (2022).

Such problems include diffusion–reaction equations, transient diffusion, incompressible viscous shear-driven Couette flow, incompressible viscous and visco-elastic Stokes equation. Remarkably, the APT method can be applied to other classes of problems, that are described in the present paper.

The present study provides a comprehensive study of the application of the APT method to compressible quasi-static elastic and visco-elastic equations and to coupled hydro-mechanical problems represented by the quasi-static Biot's poroelastic equations.

The novelties of this paper are summarized as follows:

1. A set of optimal parameters tailored for compressible quasi-static elastic and viscoelastic equations is presented.

2. Validation against analytical solutions is conducted to verify the accuracy of the APT solutions of quasi-static elasticity equations.

3. A new set of optimal parameters specifically designed for coupled hydro-mechanical problems, represented by the quasi-static Biot's poroelastic equations is introduced.

4. Applications of the APT method are presented for ultra-high resolution simulations of $10,000^2$ ~~voxels~~ in 2D and 512^3 ~~voxels~~ in 3D for poro-elastoplastic equations.

2 Mathematical formulation: quasi-static elasticity equations

2.1 General form

Consider a domain V in a three-dimensional Euclidean space E^3 bounded by a regular surface ∂V. The equilibrium equation (conservation of linear momentum under the conditions of equilibrium and neglecting body forces) is (Landau and Lifshitz, 1959; Nemat-Nasser and Hori, 2013)

$$\boldsymbol{\nabla} \cdot \boldsymbol{\sigma} = 0, \tag{1}$$

where $\boldsymbol{\sigma}$ is stress tensor, $\cdot$ is the dot product, $\boldsymbol{\nabla}$ is the del operator and $\boldsymbol{\nabla}\cdot$ is the divergence operator. The del operator, $\boldsymbol{\nabla}$, is a vectorial differential operator, denoted by Li and Wang (2008); Nemat-Nasser and Hori (2013): $\boldsymbol{\nabla} \equiv \partial_i \mathbf{e}_i \equiv \partial \mathbf{e}_i / \partial x_i$, where $\mathbf{e}_i$ are the base vectors and x_i are the coordinates. The stress tensor $\boldsymbol{\sigma}$ can be decomposed into pressure (minus the mean stress), p, and deviatoric stress tensor, $\boldsymbol{\tau}$, such that $\boldsymbol{\sigma} = -p\mathbf{I}_2 + \boldsymbol{\tau}$, where $\mathbf{I}_2$ is the second order identity tensor. In a rate formulation, the constitutive equation (the stress-rate-velocity relation) is

$$\frac{\partial \boldsymbol{\sigma}(\mathbf{v})}{\partial t} = \mathbf{C} : \frac{\partial \boldsymbol{\varepsilon}}{\partial t}, \tag{2}$$

$$\frac{\partial \boldsymbol{\varepsilon}}{\partial t} = \frac{1}{2}\left(\boldsymbol{\nabla} \otimes \mathbf{v} + (\boldsymbol{\nabla} \otimes \mathbf{v})^{\mathrm{T}}\right), \tag{3}$$

where $\mathbf{C}$ is the 4-th rank stiffness tensor (with components C_{ijkl}), ":" is the double-dot product, $\otimes$ is the tensor product, the superscript "$^{\mathrm{T}}$" denotes transpose, $\partial\boldsymbol{\varepsilon}/\partial t$ is the strain-rate tensor, $\mathbf{v}$ is the velocity field. For the elasticity problems, we consider two different tasks: (i) loading/unloading of an elastic body and (ii) calculation of effective elastic properties.

2.2 1D elasticity equations

For simplicity, we consider 1D elasticity equations~~as~~. We consider the following system of equations:

$$\begin{cases} \dfrac{\partial \sigma_{xx}}{\partial t} = (K + \frac{4}{3}G)\dfrac{\partial v_x}{\partial x} \\ 0 = \dfrac{\partial \sigma_{xx}}{\partial x}, \end{cases} \tag{4}$$

where σ_{xx} is the component of the stress tensor, v_x is the velocity, K is the bulk modulus, G is the shear modulus. Note that the system of equations (4) is a 1D version of the full system of elasticity equations (1)-(3).

2.2.1 Problem statement

The system of equations (1)-(3) can be applied to solve many problems in solid mechanics. Particularly, as an example in this study, we use these equations to solve two applied problems: (i) - loading/unloading of an elastic body and (ii) - calculation of effective elastic properties.

For the analysis of loading/unloading processes in an elastic body, the system of equations (4) is discretized with a physical time step Δt, which is intrinsically linked to specific strain increments. The loading/unloading process is simulated through a series of time increments, cumulatively spanning the total time of interest. This total time corresponds to the overall strain accumulation within the elastic body. In contrast, when computing effective elastic properties (task ii), the system of equations (4) is utilized with a single loading increment, characterized by a physical time step Δt. This solitary increment corresponds to a single strain loading step. Subsequently, the stress and strain fields are spatially averaged across the model domain. The division of these averaged quantities yields the effective elastic moduli.

2.3 The pseudo-transient method

The pseudo-transient(PT) method method is used to solve the system of ~~equation~~ equations (4) (Frankel, 1950; Räss et al., 2022). The pseudo-transient method is matrix-free and builds on a transient physics analogy to establish a stationary solution. The main idea is that the solution of a quasi-static equation (stationary process), usually described by an elliptic PDE, is represented by an attractor of a transient process described by parabolic or hyperbolic PDEs.

2.3.1 ~~The first-order PT method~~

~~Let us write the first and the simplest version of the pseudo-transient method:~~

$$\begin{cases} \dfrac{\partial \sigma_{xx}}{\partial t} = (K + \frac{4}{3}G)\dfrac{\partial v_x}{\partial x} \\ 0 = \dfrac{\partial \sigma_{xx}}{\partial x} - \mu\, v_x, \end{cases}$$

where μ is an attenuation parameter. The system of equations (A1) represents a diffusive-type physical behavior. The system is solved once the term μv_x converges to zero with a certain precision (e.g., 10^{-12}). The convergence of this type of equation is $\sim n_x^2$, where n_x is the number of grid cells in x-direction. Such convergence rate makes this method impractical for large 3D problems, therefore, this method is not analyzed here. An interested reader can find more details in Räss et al. (2022).

2.3.1 The accelerated pseudo-transient method: damping scheme 1

Now, let us consider a more advanced version of the pseudo-transient which we will call the accelerated pseudo-transient method (APT):

$$\begin{cases} \dfrac{\partial \sigma_{xx}}{\partial t} = (K + \frac{4}{3}G)\dfrac{\partial v_x}{\partial x} \\ \widetilde{\rho}\dfrac{\partial v_x}{\partial \widetilde{t}} = \dfrac{\partial \sigma_{xx}}{\partial x} - \mu v_x, \end{cases}$$

where $\widetilde{t}$ is a "pseudo" time and μ is an attenuation parameter. The system (A2) is solved once the terms $\partial v_x/\partial \widetilde{t}$ Simply put, the equations are written in their residual form, and μv_x converge to zero with pseudo-time derivatives are added to the left-hand side. The solution is achieved once the pseudo-time derivatives attenuate to a certain precision (e.g., 10^{-12}). The advantage of this system of equation (A2) over (A1) is that now the system of equation (A2) describes propagating waves (i.e., hyperbolic), and, therefore, the convergence rate is $\sim n_x$ (compare to $\sim n_x^2$ in An overview of the first-order PT method (A1)) (see Räss et al. (2022) for details). This method has been successfully applied to solve coupled two-phase flow physics represented by solitary porosity waves (Räss et al., 2019). first simplified versions of the PT and APT methods is given in in Appendix A.

2.3.1 The accelerated pseudo-transient method: modern version

2.3.2 The accelerated pseudo-transient method: damping scheme 2

Here we report a modification modern version of the APT method. The solution of the quasi-static elasticity equations can be achieved in two steps. (i) Inertial terms are added into the equations stressconstitutive relations, (ii) these terms are Inertial terms are responsible for wave propagation in pseudo physical time and space (i.e., hyperbolic) and viscous terms (treated as

a Maxwell rheology~~(a viscous damper))~~ are the physical quantities. The quasi-static elasticity equations ~~(A1) (4)~~ can then be re-written with the pseudo-time $\widetilde{t}$,

$$\begin{cases} \frac{1}{\widetilde{H}}\frac{\partial \sigma_{xx}}{\partial \widetilde{t}} + \frac{1}{H}\frac{\sigma_{xx}-\hat{\sigma}_{xx}}{\Delta t} = \frac{\partial v_x}{\partial x} \\ \widetilde{\rho}\frac{\partial v_x}{\partial \widetilde{t}} = \frac{\partial \sigma_{xx}}{\partial x}, \end{cases} \tag{5}$$

where $\hat{\sigma}_{xx}$ is the stress field at the previous physical time step and $C_{1111} = \widetilde{H} \equiv H = K + \frac{4}{3}G$ is the P-wave modulus. ~~The system (5) has to~~ For example, the system (5) can be solved for the case of elastic loading/unloading where the stress $\hat{\sigma}_{xx}$ is non-zero from the previous physical time step.

~~The~~ For the analysis of the system of equations (5) ~~can be further simplified~~ we can omit $\hat{\sigma}$ since the stress $\hat{\sigma}$ does not change inside the loop over "pseudo" time $\widetilde{t}$:

$$\begin{cases} \frac{1}{\widetilde{H}}\frac{\partial \sigma_{xx}}{\partial \widetilde{t}} + \frac{1}{H}\frac{\sigma_{xx}}{\Delta t} = \frac{\partial v_x}{\partial x} \\ \widetilde{\rho}\frac{\partial v_x}{\partial \widetilde{t}} = \frac{\partial \sigma_{xx}}{\partial x}. \end{cases} \tag{6}$$

In the system (5) (or (6)), $\widetilde{\rho}$ is a to be determined numerical parameter. For the analysis of the optimal numerical parameters, the systems of equations (5) and (6) are equivalent to each other since the quantity $\hat{\sigma}_{xx}$ is constant during the iterations over the "pseudo" time $\widetilde{t}$.

The APT version of expression (5) (or (6)) where the stress tenor is decomposed into pressure and deviatoric stress tensor is provided in Appendix B~~. A~~ , and a discrete version of the system (6) is provided in Appendix C. A Matlab routine to solve the system (6) is presented in Appendix D.

The system of equations (6) is hyperbolic and corresponds to a wave propagation in a dissipative medium. The numerical parameters in the system (6) determine the attenuation of propagating waves. Our target is to solve elasticity equations that are quasi-static. Therefore, the goal is to find optimal values of the numerical parameters that corresponds to the fastest attenuation of propagating waves. More precisely, once the "pseudo" time derivatives ($\partial \sigma_{xx}/\partial \widetilde{t}$, $\partial v_x/\partial \widetilde{t}$) in the system (6) disappear, the resulting solution of the quasi-static equations is found. In other words, the solution to quasi-static equations in an attractor of the system of equations (6) at large "pseudo"-time-scales. For a particular (optimal) choice of the numerical parameters, the attractor solution can be achieved faster than by using non-optimal values of the numerical parameters. In the best scenario, the number of iterations n_I needed to converge to the target solution is $n_I \sim n_x$, and more precisely $n_I = k\, n_x$, where usually k is in a range of $k \in [5; 50]$ (the low and upper bounds provided must be considered as an approximation). In other words, the wave travels several times throughout the whole domain before the corresponding updates of the time derivatives attenuate to a desired precision. If non-optimal parameters are used, the solution may not converge for a long computational time.

Let us describe some basic features of the system of equations (6). The “numerical" primary or P-wave velocity can be ~~calculated~~ defined as:

$$\widetilde{V}_p = \sqrt{\frac{\widetilde{H}}{\widetilde{\rho}}}. \tag{7}$$

The Courant–Friedrichs–Lewy (CFL) condition for the system of ~~equation~~ equations (6) suggest that (Alkhimenkov et al., 2021a)

$$\Delta\widetilde{t} \leq \frac{\Delta x}{\widetilde{V}_p} \qquad \text{or} \qquad \Delta\widetilde{t} = \frac{\widetilde{C}\Delta x}{\widetilde{V}_p}, \tag{8}$$

where $\widetilde{C} \leq 1$. Note that the system of equations (6) is identical to the damped linear wave equation and the CFL condition (8) is just a lower bound (Alkhimenkov et al., 2021a). It is important to mention that we do not need to know the optimal values of all the numerical parameters separately. Instead, the following combinations are needed for the numerical implementation of the APT algorithm: $\widetilde{H}\Delta\widetilde{t}$ and $\Delta\widetilde{t}/\widetilde{\rho}$.

Let us analyze the system of equations (6). First, we perform a dispersion analysis. A solution of traveling waves in dissipative media can be written as

$$fF(\widetilde{t},x) = \exp\left[\frac{(\gamma\widetilde{V}_p\widetilde{t} + \pi\omega x i)}{L_x}\right], \tag{9}$$

where γ is the amplitude, $\omega = 2\pi f$ is the angular frequency (f is the frequency), i is the imaginary unit and in our description $\exp[\cdot] \equiv e^{(\cdot)}$. The amplification matrix F of this system is a 2×2 matrix (Hirsch, 1988; Alkhimenkov et al., 2021a):

$$F = \begin{bmatrix} \dfrac{\gamma\Delta x}{L_x} & \dfrac{-3i\pi\Delta x}{7\,\mathrm{St}} \\ \dfrac{-7\,\Delta x\,\mathrm{St}\,\pi}{3\,L_x^2} & \dfrac{\Delta x\,(\mathrm{St}+\gamma)}{L_x} \end{bmatrix}, \tag{10}$$

where the dimensionless parameter, the Strouhal number, St, is expressed as

$$\mathrm{St} = \frac{L_x}{\widetilde{V}_p\,\Delta t}. \tag{11}$$

The discriminant D of the matrix (10) is

$$D = \left(\gamma^2 + \mathrm{St}\,\gamma + \pi^2\right)\left(\frac{\Delta x}{L_x}\right)^2 \tag{12}$$

Setting $D = 0$ and solving for γ, we get two roots:

$$\gamma_1 = -\frac{\mathrm{St}}{2} + \frac{\sqrt{-4\pi^2 + \mathrm{St}^2}}{2}, \tag{13}$$

$$\gamma_2 = -\frac{\mathrm{St}}{2} - \frac{\sqrt{-4\pi^2 + \mathrm{St}^2}}{2}, \tag{14}$$

The ~~minimum of real part~~ real parts of the roots γ_1 and γ_2 control the exponential decay rate of the solution (Räss et al., 2022), therefore, we are interested in the minimum of these values. This minimum reaches ~~maximal~~ its value when the discriminant is zero:

$$-4\pi^2 + \mathrm{St}^2 = 0. \tag{15}$$

The resulting solution for St has two roots: 2π and -2π. Taking the positive root we get

$$\mathrm{St} = \mathrm{St}_{\mathrm{opt}} = 2\,\pi, \tag{16}$$

which is the optimal value of the numerical parameter St that corresponds to the fastest attenuation of propagating waves.

There is only one numerical parameter that controls the dissipation and convergence to the target solution of the quasi-static equations: the Strouhal number, St, which is a purely numerical parameter in our analysis and can be chosen arbitrary. For $\mathrm{St} \ll 1$ the system of equations (6) behaves as purely hyperbolic without the stiff source term; in other words, propagating waves do not attenuate (especially when $\mathrm{St} \to 0$). Contrary, for $\mathrm{St} \gg 1$ the system of equations (6) behaves as hyperbolic with the stiff source term, that dominates; therefore, the system of equations (6) behaves as a diffusion process and attenuate very slowly. The optimal choice of the Strouhal number, St, is between these two limits: $\mathrm{St} = \mathrm{St}_{\mathrm{opt}} = 2\,\pi$ as it is shown by expression (16).

Let us do some transformations with expression (11). Our goal is to separate the numerical combination $\Delta\widetilde{t}/\widetilde{\rho}$ on the left hand side and the other variables on the right hand side:

$$1 = \frac{L_x}{\mathrm{St}\,\widetilde{V}_p\,\Delta t} \iff 1 = \frac{L_x\sqrt{\widetilde{\rho}}}{\mathrm{St}\,\sqrt{\widetilde{H}}\,\Delta t}\frac{\sqrt{\widetilde{\rho}}\Delta\widetilde{t}}{\sqrt{\widetilde{\rho}}\Delta\widetilde{t}} \iff \frac{\Delta\widetilde{t}}{\widetilde{\rho}} = \frac{L_x\Delta\widetilde{t}}{\mathrm{St}\sqrt{\widetilde{H}}\sqrt{\widetilde{\rho}}\Delta t}\frac{\widetilde{V}_p}{\widetilde{V}_p}, \tag{17}$$

and continue

$$\frac{\Delta\widetilde{t}}{\widetilde{\rho}} = \frac{\widetilde{V}_p\,\Delta\widetilde{t}\,L_x}{\mathrm{St}\,\widetilde{H}\,\Delta t}. \tag{18}$$

By using expression (8), we evaluate that $\widetilde{V}_p\,\Delta\widetilde{t} = \widetilde{C}\Delta x$, therefore, equation (18) can be rewritten as

$$\frac{\Delta\widetilde{t}}{\widetilde{\rho}} = \frac{\widetilde{C}\Delta x\,L_x}{\mathrm{St}\,\widetilde{H}\,\Delta t}. \tag{19}$$

In expression (19), all the parameters on the right hand side are known, thus $\Delta\widetilde{t}/\widetilde{\rho}$ can be evaluated. Now let us create an expression for the second numerical combination, $\widetilde{H}\Delta\widetilde{t}$. For that we employ the following transformations:

$$1 = \frac{\widetilde{V}_p^2\,\Delta\widetilde{t}^2}{\widetilde{V}_p^2\,\Delta\widetilde{t}^2} \iff \frac{\widetilde{V}_p^2\,\widetilde{\rho}\,\Delta\widetilde{t}^2}{\widetilde{H}\,\Delta\widetilde{t}^2} \iff \widetilde{H}\Delta\widetilde{t} = (\widetilde{V}_p\,\Delta\widetilde{t})^2\left(\frac{\Delta\widetilde{t}}{\widetilde{\rho}}\right)^{-1}, \tag{20}$$

Note that $\widetilde{V}_p\,\Delta\widetilde{t}$ and $\Delta\widetilde{t}/\widetilde{\rho}$ are already defined above, therefore, it is straightforward to calculate $\widetilde{H}\Delta\widetilde{t}$. Therefore, the system of equations (5) (or (6)) or its discrete version (C1) can be solved.

2.3.2 Problem statement: validation of the numerical parameters

To validate the numerical parameters, the following experiment is performed: in the numerical solver, we set all boundary conditions to zero and initialize the system with a sinusoidal wave. The numerical solution is then run over pseudo-time until it converges to a specified precision (i.e., 10^{-12}). Simultaneously, the same equation is solved using the analytical method (amplification matrix) to achieve the same precision (i.e., 10^{-12}). The results are then compared as a function of St. Ideally, the results should be identical or very close, which would validate the choice of numerical parameters and the applied numerical scheme. For the numerical solution, we use a classical conservative staggered space-time grid discretization (Virieux, 1986) which is equivalent to a finite volume approach (Dormy and Tarantola, 1995). More details on the present discretization can be found in Alkhimenkov et al. (2021b, a).

2.4 Applications of the APT method

To demonstrate the effectiveness and robustness of the APT method, we provide several applications, including the calculation of the convergence rate, the determination of effective elastic properties in homogeneous and heterogeneous media, and comparisons against analytical solutions.

2.4.1 Numerical experiment 1: convergence rate in a homogeneous medium

Figure 1 shows the numerical and analytical results for the system of equations (6) (see explanation in section 2.3.2). The numerical results correspond to the solution with different St numbers until the update of the "pseudo-time" derivatives becomes less than 10^{-9}. The analytical result corresponds to the analytical solution of the dispersion relations as a function of St. It can be seen that the analytical and numerical results are in excellent agreement (Figure 1) that validates the proposed approach.

2.4.2 Numerical experiment 2: effective properties of a homogeneous medium

Let us consider a 1D numerical domain with $L_x = 1$, which is discretized into $n_x = 1000$ grid cells. The material parameters are $K = G = 1$ and $\Delta t = 1$. For this experiment, a velocity boundary conditions are applied by prescribing $v_x(n = 1) = 1$ and $v_x(n = n_x) = 0$, where n is a grid cell number in a 1D domain ($v_x(n = 1) = 1$ means that the velocity $v_x = 1$ at the first grid cell ($n = 1$) which corresponds to the left corner of the 1D domain L_x). All other parameters and initial conditions are set to zero.

Figure 1b shows the velocity field (panel a) and the amplitudes of the stress field~~for the two damping schemes (scheme 1, where $\mu = \pi$, and scheme 2)~~. Since the medium is homogeneous, the effective elastic parameters can be calculated exactly: ~~$H^* = K + 4/3G = 7/3$~~$H^*_{an} = K + 4/3G = 7/3$. Numerically, the effective elastic parameters are calculated from the discrete values for the APT method:

$$H^*_{num} = \frac{\sum_{i=1}^{nx} [\sigma_{xx}]_i}{\sum_{i=1}^{nx} [\partial u_x / \partial x]_i}, \tag{21}$$

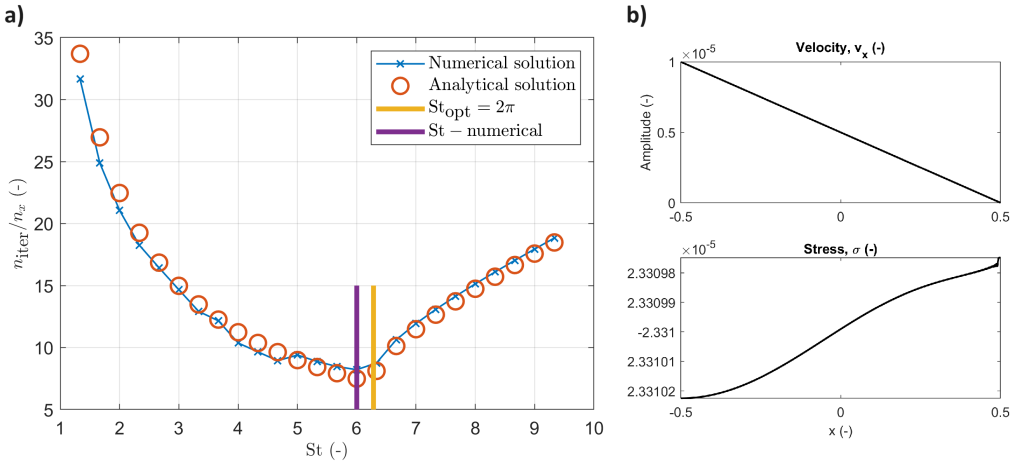

Figure 1. Panel (a): Convergence rate in a homogeneous elastic medium: numerical and analytical results as a function of the dimensionless parameter St. Panel (b): Numerical results of APT method for velocity and stress fields in the homogeneous medium for the ~~two~~ damping ~~schemes~~scheme (5). Upper panel corresponds to the velocity field ~~, middle panel shows the stress field considering damping scheme 2~~ and lower panel shows the stress field~~considering damping scheme 1.~~.

where $u_x = v_x \Delta t$. After $5\,n_x$ iterations in "pseudo-time" ~~, both damping strategies provide us with similar results: the accuracy is $\partial v_x/\partial \widetilde{t} = 10^{-13}$ for the damping scheme 1 and $\partial v_x/\partial \widetilde{t} = 10^{-14}$ for the damping scheme 2.~~ we can report the accuracy (in residuals) $dv_x = 10^{-13}$. This result correspond to the difference between the numerical value for H^* and the analytical value for $H^*_{an} = 7/3$ via $(H^*_{an} - H^*_{num})/H^*_{an} \times 100\%$ to as $10^{-12}\%$.

2.4.3 Numerical experiment 3: convergence rate in a heterogeneous medium

~~Now, let us~~ Let us again consider a 1D numerical domain with $L_x = 1$, which is discretized into $n_x = 1000$ grid cells. The boundary conditions are the same as in the previous section (Numerical experiment 2). Now, we consider a heterogeneous medium in 1D represented by layers of different elastic properties. There are ten layers with the properties $K_1 = G_1 = 1$ and $K_2 = G_2 = 0.05$. Figure 2 shows numerical results for the system of equations (6). The numerical results correspond to the solution as a function of St until the update of the "pseudo-time" derivatives becomes withing the range 10^{-9}. It can be seen that the optimal value for of St that is valid in homogeneous medium is not valid here for a heterogeneous medium. Instead, a special scaling is needed of St with a parameter A which is defined below.

2.4.4 Numerical experiment 4: effective properties of a heterogeneous medium

We perform the numerical experiment considering the ~~two damping schemes: damping schemes 1 with $\mu = \pi$ and damping schemes 2~~ damping scheme (6) as a function of St. By running a set of numerical simulations with different optimal parameters,

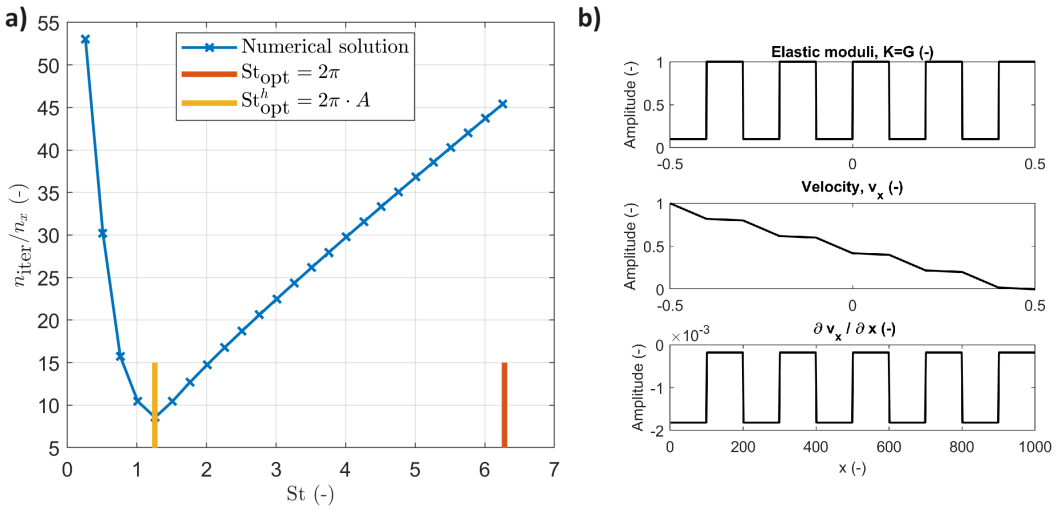

Figure 2. Panel (a): Numerical results: convergence rate in a heterogeneous medium ~~for the damping scheme 2~~ as a function of St. Panel (b): Numerical results for velocity and stress fields in a layered (heterogeneous) medium~~for the two damping schemes~~. Upper panel corresponds to variations of bulk modulus K (the same as variations in the shear modulus G)~~, middle panel shows the velocity field considering damping schemes 1 and 2.~~ Lower panel shows the spatial derivative of the velocity field~~considering damping schemes 1 and 2.~~

we found that the following re-scaling of $\mathrm{St}_{\mathrm{opt}}$ via parameter A provides the best fast convergence rate

$$\mathrm{St}^h_{\mathrm{opt}} = A \cdot \mathrm{St}_{\mathrm{opt}}, \tag{22}$$

where A is a minimum of the elastic moduli of the softest material divided by volume fraction of the weakest phase ϕ:

$$A = min(K_2, G_2)/\phi. \tag{23}$$

Figure~~Figure~~ 2 shows the distribution of elastic moduli (panel a), the velocity field and the spatial derivative of the velocity field~~for damping schemes 1 and 2. After $5n_x$~~. After $5\,n_x$ iterations in "~~pseudo~~pseudo-time"~~time, damping strategies provide us with the following results: the accuracy is $(2.5 \cdot 10^{-4})\%$ for the damping scheme 2 and 6.15% for the damping scheme 1. This experiment shows that for practical applications in heterogeneous media, damping scheme 2 provides us with a faster convergence and more accurate results than the damping scheme 1. Note that the definition of A in equation (23) is valid for the specific parameters of the medium considered here and is not universal~~, we report the following accuracy (in residuals) is $dv_x = 10^{-7}$. This results correspond to the difference between the numerical value for H^* and the analytical value for $H^*_{an} = 0.42(42)$ via $(H^*_{an} - H^*_{num})/H^*_{an} \times 100\%$ to $2 \times 10^{-3}\%$ for the damping scheme represented by equation (6).

3 Mathematical formulation: viscoelasticity

Now, let us consider viscoelastic equations. The general form is the following:

$$\begin{cases} \dfrac{1}{K}\dfrac{\partial p}{\partial t} = -\nabla\cdot\mathbf{v} \\ \dfrac{1}{2G}\dfrac{\partial \boldsymbol{\tau}}{\partial t} + \dfrac{\boldsymbol{\tau}}{2\mu_s} = \boldsymbol{\varepsilon} - \dfrac{1}{3}(\nabla\cdot\mathbf{v})\mathbf{I}_2 \\ 0 = \nabla\cdot(-p\mathbf{I}_2 + \boldsymbol{\tau}), \end{cases} \tag{24}$$

where μ_s is the shear viscosity of the solid material, p is the pressure, $\boldsymbol{\tau}$ is the deviatoric stress tensor ($\sigma = -p\mathbf{I}_2 + \boldsymbol{\tau}$. The system of equations ~~(4)~~ (24) can be re-written for calculation of effective viscoelastic properties in 1D as

$$\begin{cases} \dfrac{1}{K}\dfrac{\partial p}{\partial t} = -\dfrac{\partial v_x}{\partial x} \\ \dfrac{1}{2G}\dfrac{\partial \tau_{xx}}{\partial t} + \dfrac{\tau_{xx}}{2\mu_s} = \left(\dfrac{\partial v_x}{\partial x} - \dfrac{1}{3}\dfrac{\partial v_x}{\partial x}\right) \\ 0 = \dfrac{\partial(-p+\tau_{xx})}{\partial x}, \end{cases} \tag{25}$$

~~where μ_s is the (physical) viscosity of the solid material.~~

3.1 ~~Naive~~ APT scheme for viscoelastic equations

The advantage of this naive APT scheme is that there are minimal modifications to the original formulation of the APT method for elasticity equations presented in the previous sections. The system of equations (25) can be re-written as the APT scheme 2:

$$\begin{cases} \dfrac{1}{\widetilde{K}}\dfrac{\partial p}{\partial \widetilde{t}} + \dfrac{1}{K}\dfrac{p-\hat{p}}{\Delta t} = -\dfrac{\partial v_x}{\partial x} \\ \dfrac{1}{2\widetilde{G}}\dfrac{\partial \tau_{xx}}{\partial \widetilde{t}} + \dfrac{1}{2G}\dfrac{\tau_{xx}-\hat{\tau}_{xx}}{\Delta t} + \dfrac{\tau_{xx}}{2\mu_s} = \left(\dfrac{\partial v_x}{\partial x} - \dfrac{1}{3}\dfrac{\partial v_x}{\partial x}\right) \\ \widetilde{\rho}\dfrac{\partial v_x}{\partial \widetilde{t}} = -\dfrac{\partial \sigma_{xx}}{\partial x}, \end{cases} \tag{26}$$

~~where~~

where

$$\frac{\Delta\widetilde{t}}{\widetilde{\rho}} = \frac{\widetilde{V}_p\,\Delta\widetilde{t}\,L_x}{\mathrm{St}\,H^{\mathrm{ve}}}, \tag{27}$$

and $\widetilde{H}^{\mathrm{ve}}$ is defined as

$$H^{\mathrm{ve}} = \left((K\,\Delta t + \frac{4}{3} G^{\mathrm{ve}}) \right)^{-1}, \tag{28}$$

In other words, in the viscoelastic scenario we replaced "elastic" modulus H by the viscoelastic one $\widetilde{H}^{\mathrm{ve}}$ represented by equation (28). All other numerical parameters remains the same as in single-phase elasticity equation. The resulting solution for St has three roots. Let us assume that $K = G = \mu_s$. The positive root is

$$\mathrm{St}{=}\mathrm{St}_{\mathrm{opt}} = 11.469\,G + 4.915,$$

where

$$G^{\mathrm{ve}} = \left(\frac{1}{\mu_s} + \frac{1}{G\Delta t} \right)^{-1} \tag{29}$$

which is the optimal value of the numerical parameter St that corresponds to the fastest attenuation of propagating waves. If $G = 1$, then

$$\mathrm{St}{=}\mathrm{St}_{\mathrm{opt}} = 11.469\,G + 4.915 = 16.38.$$

A discrete version of the system (26) is provided in Appendix E. A similarity with the analysis proposed by Räss et al. (2022) is provided in the discussion section. Note that the optimal value of $\mathrm{St}_{\mathrm{opt}}$ must be re-evaluated for the specific parameters of the medium.

Convergence rate in a homogeneous viscoelastic medium: numerical and analytical results as a function of the dimensionless parameter St.

3.2 Elegant APT scheme

Let us simplify the is the apparent "viscoelastic" shear modulus. Let us modify the scheme (26) by re-arranging terms and removing omitting quantities that are constant during the iterations over $\widetilde{t}$:

$$\begin{cases} \dfrac{1}{\widetilde{K}} \dfrac{\partial p}{\partial \widetilde{t}} + \dfrac{1}{K} \dfrac{p}{\Delta t} = -\dfrac{\partial v_x}{\partial x} \\ \dfrac{1}{2\widetilde{G}} \dfrac{\partial \tau_{xx}}{\partial \widetilde{t}} + \dfrac{\tau_{xx}}{2} \left(\dfrac{1}{G\Delta t} + \dfrac{1}{\mu_s} \right) = \left(\dfrac{\partial v_x}{\partial x} - \dfrac{1}{3} \dfrac{\partial v_x}{\partial x} \right) \\ \widetilde{\rho} \dfrac{\partial v_x}{\partial \widetilde{t}} = -\dfrac{\partial \sigma_{xx}}{\partial x}. \end{cases} \tag{30}$$

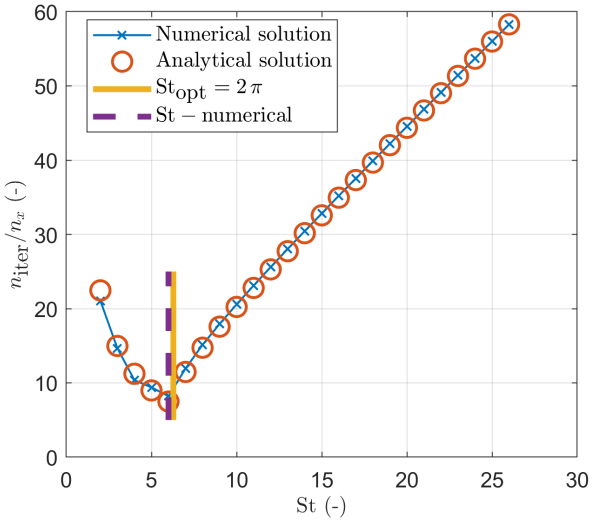

Figure 3. Convergence rate in a homogeneous viscoelastic medium: numerical and analytical results as a function of the dimensionless parameter St.

Further simplifications leads to the following system:

$$\begin{cases} \dfrac{1}{\widetilde{K}}\dfrac{\partial p}{\partial \widetilde{t}} + \dfrac{1}{K}\dfrac{p}{\Delta t} = -\dfrac{\partial v_x}{\partial x} \\ \dfrac{1}{2\widetilde{G}}\dfrac{\partial \tau_{xx}}{\partial \widetilde{t}} + \dfrac{\tau_{xx}}{2}\dfrac{1}{G^{\mathrm{ve}}} = \left(\dfrac{\partial v_x}{\partial x} - \dfrac{1}{3}\dfrac{\partial v_x}{\partial x}\right) \\ \widetilde{\rho}\dfrac{\partial v_x}{\partial \widetilde{t}} = -\dfrac{\partial \sigma_{xx}}{\partial x} \end{cases} . \tag{31}$$

~~where~~

$$G^{\mathrm{ve}} = \left(\frac{1}{G\Delta t} + \frac{1}{\mu_s}\right)^{-1}$$

~~is the apparent "viscoelastic" shear modulus.~~ Note that (e.g., assuming $G^{\mathrm{ve}} = G$) the present system (31) becomes identical to the system (B4) (or (6)) which corresponds to the elasticity equations. Therefore, all the analysis presented for elasticity equations in the previous sections can be applied to the viscoelastic equations. If $K = G^{\mathrm{ve}} = 1$, then

$$\mathrm{St}_{\mathrm{opt}} = 2\pi, \tag{32}$$

which is the same value as in the case of the elasticity equations. It can be seen that the analytical and numerical results are in excellent agreement (Figure 3) that validates the proposed approach.

4 Mathematical formulation: coupled hydro-mechanics — quasi-static poroelasticity

The first order velocity-stress system of Biot's equations in 1D can be written as (Biot, 1962)

$$\begin{pmatrix} \dfrac{\partial \bar{p}}{\partial t} \\ \dfrac{\partial p_f}{\partial t} \end{pmatrix} = -K_u \begin{pmatrix} 1 & B \\ B & \dfrac{B}{\alpha} \end{pmatrix} \begin{pmatrix} \dfrac{\partial v_x^s}{\partial x} \\ \dfrac{\partial q_x^D}{\partial x} \end{pmatrix}, \tag{33}$$

$$\frac{\partial \bar{\tau}_{xx}}{\partial t} = 2G_u \left(\frac{\partial v_x}{\partial x} - \frac{1}{3} \frac{\partial v_x}{\partial x} \right) \tag{34}$$

and

$$\begin{pmatrix} 0 \\ 0 \end{pmatrix} = \begin{pmatrix} \dfrac{\partial(-p + \tau_{xx})}{\partial x} \\ \dfrac{\eta_f}{k} q_x^D + \dfrac{\partial p_f}{\partial x} \end{pmatrix}, \tag{35}$$

The list of symbols is given in Table 1. From the general principles of thermodynamic, the matrices of coefficients in expression (33) must be positive definite. For simplicity, expressions (33) and (34) can be combined, leading to

$$\begin{pmatrix} \dfrac{\partial \bar{\sigma}_{xx}}{\partial t} \\ -\dfrac{\partial p_f}{\partial t} \end{pmatrix} = \begin{pmatrix} K_u + \frac{4}{3} G_u & K_u B \\ K_u B & \dfrac{K_u B}{\alpha} \end{pmatrix} \begin{pmatrix} \dfrac{\partial v_x^s}{\partial x} \\ \dfrac{\partial q_x^D}{\partial x} \end{pmatrix}, \tag{36}$$

where $\bar{\sigma}_{xx} = -\bar{p} + \bar{\tau}_{xx}$. For an isotropic material saturated with a single fluid, in which the solid frame consists of a single isotropic mineral, the Biot-Willis coefficient is

$$\alpha = 1 - \frac{K_d}{K_s} \tag{37}$$

and the Skempton coefficient, B, is

$$B = \frac{1/K_d - 1/K_s}{1/K_d - 1/K_s + \phi(1/K_f - 1/K_s)}. \tag{38}$$

Other useful parameters include the undrained bulk modulus, K_u,

$$K_u = K_d \left(1 - \alpha B\right)^{-1} \equiv K_d + \alpha^2 M, \tag{39}$$

and the fluid storage coefficient, M,

$$M = K_u B / \alpha. \tag{40}$$

Equaition (39) is known as Gassmann's equation for fluid-saturated bulk modulus (Gassmann, 1951; Alkhimenkov, 2023).

Table 1. List of Symbols

Symbol	Meaning
σ^s, σ^f	solid and fluid stress
$\bar{\sigma}$	$= (1-\phi)\sigma^s + \phi\sigma^f$, total stress
p_s, p_f	solid and fluid pressure
$\bar{p}$	$= (1-\phi)p_s + \phi p_f$, total pressure
$\bar{\tau}_{xx}$	total deviatoric stress
v^s, v^f	solid and fluid velocity
q^D	$= \phi(v^f - v^s)$, Darcy velocity
ρ^s, ρ^f	solid and fluid density
ρ_t	$= (1-\phi)\rho_s + \phi\rho_f$, total density
K_s, K_f	elastic solid and fluid bulk modulus
$G_s, G_d = G_u$	elastic solid, drained and undrained shear modulus
K_d, K_u	elastic drained and undrained bulk modulus
η_f	fluid shear viscosity
k	medium permeability
ϕ	medium porosity
α	Biot-Willis coefficient
B	Skempton coefficient

4.1 APT method for the quasi-static Biot's poroelastic equations

Let us write the APT method ~~(scheme 2)~~ for the quasi-static Biot's poroelastic equations (33)-(35):

$$\begin{pmatrix} \frac{1}{\widetilde{K}_1}\frac{\partial \bar{p}}{\partial \widetilde{t}} \\ \frac{1}{\widetilde{K}_2}\frac{\partial p_f}{\partial \widetilde{t}} \end{pmatrix} + \frac{1}{K_u}\begin{pmatrix} \frac{\bar{p}-\hat{\bar{p}}}{\Delta t} \\ \frac{p_f-\hat{p}_f}{\Delta t} \end{pmatrix} = -\begin{pmatrix} 1 & B \\ B & \frac{B}{\alpha} \end{pmatrix}\begin{pmatrix} \frac{\partial v^s}{\partial x} \\ \frac{\partial q^D}{\partial x} \end{pmatrix}, \tag{41}$$

where $\hat{\bar{p}}$ and $\hat{p}_f$ are the total and fluid pressures at the previous physical time step, ~~$\widetilde{K}_1 = \widetilde{K}_2 = K_u$~~ $\widetilde{K}_1 = K_u$. For the total deviatoric stress the corresponding equation is

$$\frac{1}{2\widetilde{G}_1}\frac{\partial \overline{\tau}_{xx}}{\partial \widetilde{t}} + \frac{1}{2G_u}\frac{\overline{\tau}_{xx}-\hat{\overline{\tau}}_{xx}}{\Delta t} = \left(\frac{\partial v_x}{\partial x} - \frac{1}{3}\frac{\partial v_x}{\partial x}\right), \tag{42}$$

where $\hat{\overline{\tau}}_{xx}$ is the total stress deviator at the previous physical time step and $\widetilde{G}_1 = G_u$. The system of ~~equation~~ equations (35) is re-written as

$$\begin{pmatrix} \widetilde{\rho}_t & 0 \\ 0 & \widetilde{\rho}_a \end{pmatrix}\begin{pmatrix} \frac{\partial v_i^s}{\partial \widetilde{t}} \\ -\frac{\partial q_i^D}{\partial \widetilde{t}} \end{pmatrix} = \begin{pmatrix} \frac{\partial(-p+\tau_{xx})}{\partial x} \\ \frac{\eta_f}{k}q_i^D + \frac{\partial p_f}{\partial x} \end{pmatrix}, \tag{43}$$

where $\widetilde{\rho}_t$ and $\widetilde{\rho}_a$ are to be determined numerical parameters. A discrete form of the system of equations (41)-(43) is presented in Appendix F. In summary, we need the following combinations of the numerical parameters to effectively solve the system of equations (41)-(43): $\widetilde{K}_1\Delta\widetilde{t}$, $\widetilde{K}_2\Delta\widetilde{t}$, $\widetilde{G}_u\Delta\widetilde{t}$, $\Delta\widetilde{t}/\widetilde{\rho}_t$ and $\Delta\widetilde{t}/\widetilde{\rho}_a$. A dispersion analysis of equations (41)-(43) leads to the system of 5 equations. Without the loss of generality, we analyze the APT method of the expressions (36) and (35) which corresponds to the system of 4 equations in the dispersion analysis.

The "numerical" primary or P-wave velocity of the system of equations (41)-(43) varies as a function of I_2, which is a non-dimensional parameter:

$$I_2 = \frac{\eta_f}{k}\widetilde{\rho}_a\tau^*, \tag{44}$$

where τ^* is a characteristic time. The physical meaning of I_2 is the following: I_2 controls the behavior of the Biot's slow wave, if $I_2 \gg 1$ the slow wave behaves as a propagating wave, if $I_2 \ll 1$ the slow wave behaves as a diffusive mode. For details on the non-dimensional analysis of these equations we refer to Alkhimenkov et al. (2021b). The CFL condition for the system of ~~equation~~ equations (41)-(43) suggest that (Alkhimenkov et al., 2021a)

$$\Delta\widetilde{t} \leq \frac{\Delta x}{\widetilde{V}_p^{HF}} \qquad \text{or} \qquad \Delta\widetilde{t} = \frac{\widetilde{C}\Delta x}{\widetilde{V}_p^{HF}}, \tag{45}$$

where $\widetilde{V}_p^{HF}$ is the "numerical" P-wave velocity at high frequencies and $\widetilde{C} \leq 1$. Note that $\widetilde{V}_p^{HF} > \widetilde{V}_p^{LF}$, where the latter is the "numerical" P-wave velocity at low frequencies. Since the exact expression for $\widetilde{V}_p^{HF}$ is cumbersome, we can modify the CFL

condition (45) as

$$\Delta\widetilde{t} = \frac{\widetilde{C}\Delta x}{\widetilde{V}_p^{LF}}, \tag{46}$$

where

$$\widetilde{V}_p^{LF} = \sqrt{\frac{\widetilde{K}_1 + \frac{4}{3}\widetilde{G}_1}{\widetilde{\rho}}} = \sqrt{\frac{K_u + \frac{4}{3}G_u}{\widetilde{\rho}}} = \sqrt{\frac{H_u}{\widetilde{\rho}}}, \tag{47}$$

where $H_u = K_u + \frac{4}{3}G_u$ is the undrained P-wave modulus. The reason for setting $\widetilde{K}_1 = K_u$ and $\widetilde{G}_1 = G$ is simplicity, since the 4-th order equation has only two degrees of freedom for the APT method's parameters choice, a different choice of these parameters would simply re-scale the two final optimal parameters.

4.1.1 The choice of the numerical parameters

The analysis here is similar to that one for a single-phase media. From the stability analysis (46), we evaluate that

$$\widetilde{V}_p^{LF}\,\Delta\widetilde{t} = \widetilde{C}\Delta x. \tag{48}$$

Let us introduce a dimensionless parameter, the Strouhal number (St) which is expressed as

$$\mathrm{St} = \frac{L_x}{\widetilde{V}_p^{LF}\,\Delta t}. \tag{49}$$

By analogy with expression (17), we write the formula for the first numerical combination:

$$\frac{\Delta\widetilde{t}}{\widetilde{\rho}_t} = \frac{\widetilde{V}_p^{LF}\,\Delta\widetilde{t}\,L_x}{\mathrm{St}\,H_u\,\Delta t}. \tag{50}$$

The second numerical combination is

$$\widetilde{G}_1\Delta\widetilde{t} = \frac{(\widetilde{V}_p^{LF}\,\Delta\widetilde{t})^2}{(r+\frac{4}{3})}\left(\frac{\Delta\widetilde{t}}{\widetilde{\rho}_t}\right)^{-1}, \tag{51}$$

where $r = K_u/G_u$. Note that $\widetilde{V}_p^{LF}\,\Delta\widetilde{t}$ and $\Delta\widetilde{t}/\widetilde{\rho}_t$ are already defined above, therefore, it is straightforward to calculate $\widetilde{G}_1\Delta\widetilde{t}$. Calculation of $\widetilde{K}_1\Delta\widetilde{t}$ is also straightforward: $\widetilde{K}_1\,\Delta\widetilde{t} = r\,\widetilde{G}_1\,\Delta\widetilde{t}$. The next numerical combination $\widetilde{K}_2\Delta\widetilde{t}$ is

$$\widetilde{K}_2\Delta\widetilde{t} = (\widetilde{V}_p^{LF}\,\Delta\widetilde{t})^2\left(\frac{\widetilde{V}_p^{LF}\,\Delta\widetilde{t}\,L_x}{\mathrm{St}\,K_u\,B/\alpha\Delta t}\right)^{-1}, \tag{52}$$

For the last combination $\Delta\widetilde{t}/\widetilde{\rho}_a$, we explore the discrete system of equations and find that

$$\frac{\Delta\widetilde{t}}{\widetilde{\rho}_a} = \frac{\Delta\widetilde{t}}{\widetilde{\rho}_t}\frac{\eta_f}{k}. \tag{53}$$

Now, the system of equations (41)-(43) can be solved.

In order to find the optimal values of St, we perform the same dispersion analysis as for a single phase media. A solution of traveling waves in dissipative media is

$$f\widetilde{F}(\widetilde{t},x) = \exp\left[\frac{(\gamma \widetilde{V}_p^{LF}\widetilde{t} + \pi\,\omega\, x\, i)}{L_x}\right], \tag{54}$$

~~where γ is the amplitude, $\omega = 2\,\pi\, f$ is the angular frequency (f is the frequency), i is the imaginary unit and in our description $\exp[\cdot] \equiv e^{(\cdot)}$.~~ A dispersion analysis of the system of equations (36) and (35) leads to a 4×4 amplification matrix. The discriminant of this matrix has four roots. The optimal value of St that corresponds to the fastest attenuation of propagating waves depends on the parameter I_2. Let us consider two end-member scenarios for values of I_2, which are explored in the next section.

4.1.2 Approximation: reduced order equations

To find the optimal values of optimal parameters for the system of equations (41)-(43) a solution of 5-th order (or 4-th order) polynomial is required. However, if we neglect the coupling in the stress-strain relation, we arrive to a 4-th order (consider only the 4-th order polynomial for simplicity) polynomial where the roots can be easily separated: two roots are the same as for single-phase elastic media and the other two roots are more complicated and belong to Darcy's law.

Lets us assume a particular value of coupling parameters: $B = 0$ and B/α and I_2as a variables ($\Delta x = 1$). The discriminant D of the matrix amplification matrix that corresponds to expressions (36) and (35) is (see also Maple file):

$$D = \frac{3}{7St + 3I_2}[((7St)/3 + I_2)\gamma^2 + (7/3St^2 + I_2 StB/\alpha + I_2)\gamma + B/\alpha St((\pi B/\alpha)^2 + I_2)](\pi^2 + St\gamma + \gamma^2). \tag{55}$$

Setting $D = 0$ and solving for γ, we get 4 roots. Two of them correspond to the term $(\pi^2 + St\gamma + \gamma^2)$ and are the same as for single-phase media:

$$\gamma_1 = -\frac{\mathrm{St}}{2} + \frac{\sqrt{-4\pi^2 + \mathrm{St}^2}}{2}, \tag{56}$$

$$\gamma_2 = -\frac{\mathrm{St}}{2} - \frac{\sqrt{-4\pi^2 + \mathrm{St}^2}}{2}, \tag{57}$$

We are interested when the discriminant is zero: $-4\pi^2 + \mathrm{St}^2 = 0$. The resulting solution for St has two roots: 2π and -2π. Taking the positive root we get

$$\mathrm{St} = \mathrm{St}_{\mathrm{opt}} = 2\,\pi, \tag{58}$$

which is the optimal value of the numerical parameter St that corresponds to the fastest attenuation of propagating waves for $I_2 \ggg 1$. For $I_2 \lll 1$ the corresponding roots are cumbersome (while have an explicit formulation: $\mathrm{St}_{\mathrm{opt}} = 4.11$), therefore, we refer an interested reader to the Maple script.

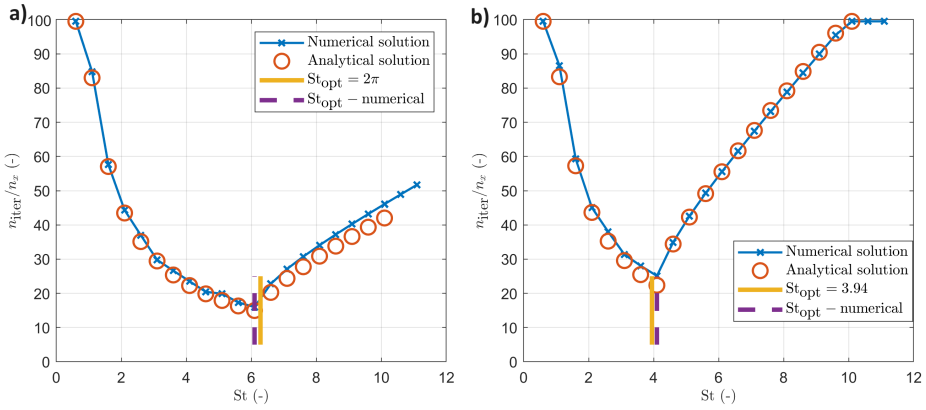

Figure 4. Panel (a): Convergence rate in a homogeneous poroelastic medium for $I_2 = 1000$: numerical and analytical results as a function of the dimensionless parameter St. Panel (b): Convergence rate in a homogeneous poroelastic medium for $I_2 = 0.001$: numerical and analytical results as a function of the dimensionless parameter St.

4.2 APT method: general case

Lets us assume a particular value of coupling parameters: $B = 5/8$ and $\alpha = 0.5$ (which corresponds to $B/\alpha = 5/4$) and we will vary I_2 from low to high values.

4.2.1 APT method for $I_2 \ggg 1$

Figure 4a shows the numerical and analytical results for the system of equations (41)-(43) for $I_2 = 1000$ (see explanation in section 2.3.2). The numerical results correspond to the solution with different St numbers until the update of the "pseudo-time" derivatives becomes less than 10^{-11}. The analytical result corresponds to the analytical solution of the dispersion relations as a function of St. It can be seen that the analytical and numerical results are in excellent agreement (Figure 4a) that validates the proposed approach. Here $\mathrm{St}_{\mathrm{opt}}$ is

$$\mathrm{St} = \mathrm{St}_{\mathrm{opt}} \approx 2\pi. \tag{59}$$

4.2.2 APT method for $I_2 \lll 1$

Figure 4b shows the numerical and analytical results for the system of equations (41)-(43) for $I_2 = 0.001$ (see explanation in section 2.3.2). The numerical results correspond to the solution with different St numbers until the update of the "pseudo-time" derivatives (i.e., residual) becomes less than ~~10^{-11}~~ 10^{-10}. The analytical result corresponds to the analytical solution of the dispersion relations as a function of St. It can be seen that the analytical and numerical results are in a good agreement (Figure 4b) that validates the proposed approach. Here $\mathrm{St}_{\mathrm{opt}}$ is

$$\mathrm{St} = \mathrm{St}_{\mathrm{opt}} \approx 2.93.94. \tag{60}$$

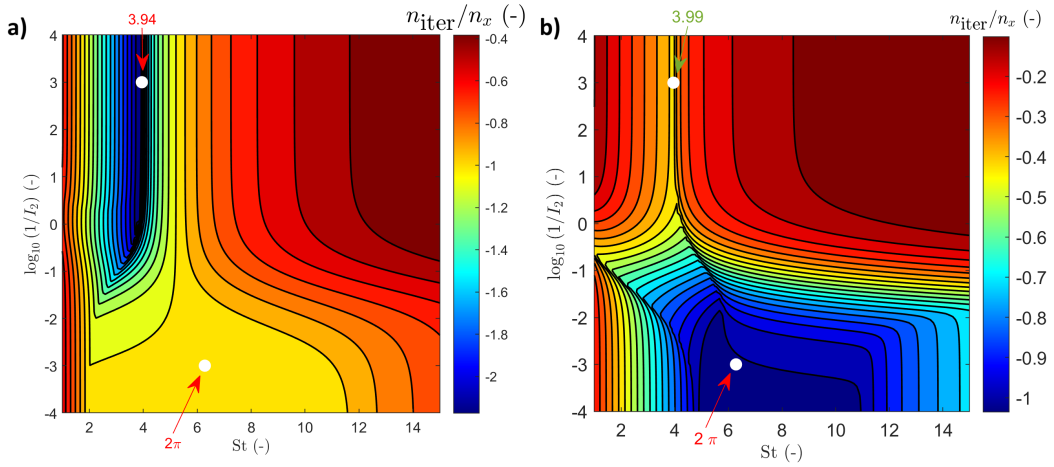

Figure 5. Convergence rate in a homogeneous poroelastic medium as a two-dimensional plot: analytical results as a function of the dimensionless parameter St and I_2. ~~The~~ In panel (a) the two white circles correspond to the values of St obtained via expressions (59) and (60). Panel (a): $B = 5/8$, $B/\alpha = 5/4$. Panel (b): $B = 1/10$, $B/\alpha = 2/10$.

Figure 5 shows the analytical results for the system of equations (41)-(43) as a function of the dimensionless parameter St and I_2 (by varying η_f/k only). Note that the optimal value of St depends on the ~~value~~ values: I_2, B and B/α.

4.2.3 ~~Approximation: reduced order equations~~

~~To find the optimal values of optimal parameters for the system of equations (41)-(43) a solution of 5-th order (or 4-th order) polynomial is required. However, if we neglect the coupling in the stress-strain relation, we arrive to a 4-th order (consider only the 4-th order polynomial for simplicity) polynomial where the roots can be easily separated: two roots are the same as for single-phase elastic media and the other two roots are more complicated and belong to Darcy's law.~~

~~The discriminant D of the matrix amplification matrix that corresponds to expressions (36) and (35) is~~

$$D = \frac{3}{14StI_2 + 6}[((14StI_2)/3 + 2)\gamma^2 + (14/3St^2I_2 + 2St + 2)\gamma + St(\pi^2 I_2 + 2)]\cdot$$

$$\cdot(\pi^2 + St\gamma + \gamma^2).$$

~~Setting $D = 0$ and solving for γ, we get 4 roots. Two of them correspond to the term $(\pi^2 + St\gamma + \gamma^2)$ and are the same as for single-phase media:~~

$$\gamma_1 = -\frac{\mathrm{St}}{2} + \frac{\sqrt{-4\pi^2 + \mathrm{St}^2}}{2},$$

$$\gamma_2 = -\frac{\mathrm{St}}{2} - \frac{\sqrt{-4\pi^2 + \mathrm{St}^2}}{2},$$

~~We are interested when the discriminant is zero: $-4\pi^2 + \mathrm{St}^2 = 0$. The resulting solution for St has two roots: 2π and -2π. Taking the positive root we get~~

$$\mathrm{St}{=}\mathrm{St}_{\mathrm{opt}} = 2\,\pi,$$

~~which is the optimal value of the numerical parameter St that corresponds to the fastest attenuation of propagating waves for $I_2 \ggg 1$.~~

~~The two other roots are are cumbersome. However, a precise analytical evaluation is possible for any value of I_2. The optimal parameters for the system of equations (41)-(43) for $I_2 \lll 1$ is different from 2π as can be seen in a 2D plot (Figure 5):~~

$$\mathrm{St}{=}\mathrm{St}_{\mathrm{opt}} \approx 2.9.$$

In summary, for practical purposes there is not need to always solve a 4-th (or 5-th) order polynomial for each set of input parameters of the quasi-static Biot's poroelastic equations. In some cases, an average of two parameters can be taken

$$\mathrm{St} = \mathrm{St}_{\mathrm{opt}} \approx (2\,\pi + 2.93.94)/2 \approx 4.59655.11. \tag{61}$$

4.2.3 2D ~~and 3D~~ numerical simulations: poroelasticity

The accuracy of the proposed ~~$\mathrm{St}_{\mathrm{opt}} \approx 2.9$~~ $\mathrm{St}_{\mathrm{opt}}$ is illustrated numerically in 2D (Figure 6a-b)~~and in 3D (Figure 6c-d)~~. It can be seen that the results presented here for 1D need some calibration to be applied to 2D ~~and 3D~~ simulations. Note that the numerical parameters are sensitive to boundary and initial conditions, which is explored below. Therefore, some test must be performed for each numerical setup.

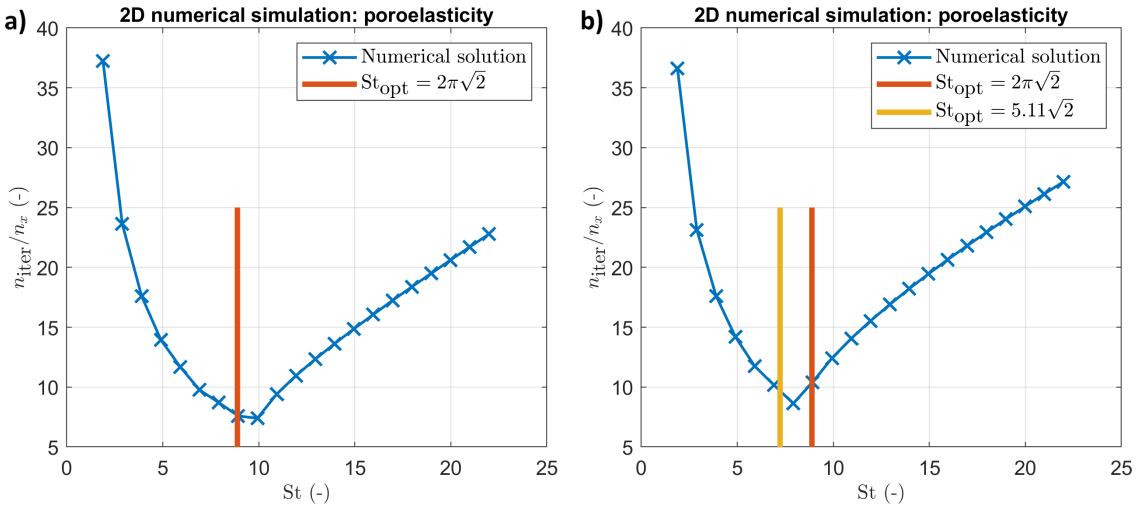

Figure 6. ~~Panel (a):~~ Convergence rate in a homogeneous poroelastic medium for ~~$I_2 = 100$~~different I_2: numerical result as a function of the dimensionless parameter St. Panel (~~b): Convergence rate in a~~~~homogeneous poroelastic medium for $I_2 = 0.01$: numerical result as a function of the dimensionless parameter St. Panel (c~~): ~~Convergence rate in a homogeneous poroelastic medium for~~ $I_2 = 100$~~: numerical result as a function of the dimensionless parameter St~~. Panel (db): ~~Convergence rate in a homogeneous poroelastic medium for~~ $I_2 = 0.01$~~: numerical result as a function of the dimensionless parameter St~~.

5 Applications: Strain Localization in Poro-Elastoplastic Media

The purpose of this section is to demonstrate the applicability of the APT method for ultra-high resolution simulations with heterogeneous initial conditions. We address the nonlinear mechanical problem of strain localization in both 2D and 3D contexts, employing an elasto-viscoplastic rheological model. This model is grounded in a hypoelastic-based constitutive framework that accommodates the simulation of large strains. The modeling process follows the formulation of incremental constitutive equations, ensuring the objectivity of the rate fields. In this study, we utilize the Jaumann-Zaremba rate to manage the time-dependent fields.

5.1 Implementation using Graphical Processing Units (GPUs)

The initial code prototyping was conducted on a laptop equipped with a 13th Gen Intel Core i9-13900HX CPU (64GB RAM) and an NVIDIA GeForce RTX 4090 (16 GB) laptop GPU. For large-scale 3D simulations, the computations were carried out on an NVIDIA DGX-1-like node, featuring 4 NVIDIA Ampere A100 GPUs (each with 80 GB of memory) and an AMD EPYC 7742 server processor with 512 GB of RAM.

5.2 Plasticity Implementation

The plasticity model adheres to a consistent poro-elasto-viscoplastic framework, with the yield function defined as

$$F(\tau, p_e) = \sqrt{J_2} - Ap_e - Bc - \eta^{\mathrm{vp}}\dot{\lambda}, \tag{62}$$

where η^{vp} represents the viscosity of the damper, $p_e = \bar{p} - p_f$ is the effective pressure. The yield function specified by equation (62) is rate-dependent Duretz et al. (2019). The plastic potential Q is expressed as

$$Q(\tau, p_e) = \sqrt{J_2} - Cp_e. \tag{63}$$

Here, the constants A, B, and C are defined as $A = \sin(\phi)$, $B = \cos(\phi)$, and $C = \sin(\psi)$, where ϕ denotes the internal friction angle, and $\psi \leq \phi$ is the dilation angle (with $\psi = 0$ for simplicity in this case).

In the numerical solver, plasticity is implemented through the following steps: (1) Compute the components of the trial deviatoric stresses $\bar{\tau}_{ij}^{\mathrm{trial}}$. (2) Using these components, calculate the trial second invariant of the deviatoric stresses, J_2^{trial}. (3) Evaluate F^{trial} using the expression

$$F^{\mathrm{trial}} = \sqrt{J_2^{\mathrm{trial}}} - (Ap_e + Bc)\,. \tag{64}$$

When the material remains in the plastic regime, the components of the trial deviatoric stresses, $\bar{\tau}_{ij}^{\mathrm{trial}}$, are re-scaled according to

$$\bar{\tau}_{ij}^{\mathrm{new}} = \bar{\tau}_{ij}^{\mathrm{trial}} \left(1 - \frac{F^{\mathrm{trial}} \Delta t G_u}{\sqrt{J_2}(\Delta t G_u + \eta^{\mathrm{vp}})}\right), \tag{65}$$

This re-scaling procedure occurs within the pseudo-transient iteration loop, and the process repeats until the components of the updated trial deviatoric stresses, $\bar{\tau}_{ij}^{\mathrm{new}}$, satisfy the condition $F^{\mathrm{trial}} = 0$, and no further re-scaling is needed. This approach is

equivalent to the standard formulation involving the plastic multiplier. An interested reader may refer to Alkhimenkov et al. (2024a, b) for more details on the implementation of plasticity.

5.3 2D Results: Ultra-High Resolution Simulations

Let us consider a 2D numerical domain with $L_x = L_y = 1$. In this set of simulations, pure shear kinematics are imposed at the boundaries of the domain, corresponding to compression along the x-axis and extension along the y-axis. The model is initialized with pre-stresses of $\bar{\tau}_{xx} = 0.0180$, $\bar{\tau}_{yy} = -0.0180$, and $\bar{\tau}_{xy} = 0$, while the fluid pressure p_f is set to zero, and the cohesion c is defined as 0.0101. The total pressure in the background material is $\bar{p} = 0.018$, with a circular anomaly located at the center of the model where the pressure is reduced to $\bar{p} = 0.005$ (Figure 7). The radius of this anomaly is $1/8$ of the domain size. The simulation is performed over 14 loading increments. The poroelastic properties of the background material are: $\alpha = 0.2958$, $B = 0.0833$, $G_d = 1$, $K_d = 1$, and $\eta_f/k = 10^{-2}$. The porosity, or fluid volume fraction, is $\phi = 0.3$, and the internal friction angle is $\varphi = 30^\circ$.

Figure 8 shows the results of the 2D simulation with an ultra-high resolution of $N = 10,239^2$ grid cells. The finite thickness of the shear bands confirms that the simulation is mesh-independent as it has been shown by Alkhimenkov et al. (2024b). The zoomed-in panels reveal extremely detailed features of the strain localization pattern. The simulation time takes about a few hours.

5.4 3D Results: Ultra-High Resolution Simulations

Let us consider a 3D numerical domain with $L_x = L_y = L_z = 1$. We present 3D results showcasing the spontaneous formation of shear bands under pure shear deformation, initiated by a spherical pressure anomaly (Figure 9a-b). These 3D simulations further validate the versatility of the APT approach (Figure ??9c-d), demonstrating its robustness in predicting poro-elastoplastic deformation and capturing brittle failure.

The boundary conditions are defined by compression along the x-axis, a slight (1%) compression along the y-axis, and extension along the z-axis. The model is initialized with pre-stresses of $\bar{\tau}_{xx} = -0.0098$, $\bar{\tau}_{yy} = -9.8\times10^{-05}$, and $\bar{\tau}_{zz} = 0.0098$, while the shear stress components $\bar{\tau}_{xy}$, $\bar{\tau}_{xz}$, and $\bar{\tau}_{yz}$ are set to zero. The fluid pressure p_f is zero, cohesion c is 0.0101, and the ratio η_f/k is set at 100. The total pressure in the background material is $\bar{p} = 0$, with a spherical anomaly located at the center of the model where the pressure is increased to $\bar{p} = 0.005$. The radius of this anomaly is $1/8$ of the domain size. The poroelastic properties of the background material are: $\alpha = 0.2958$, $B = 0.0833$, $G_d = 1$, $K_d = 1$, and $\eta_f/k = 10^2$. The porosity is $\phi = 0.3$, the internal friction angle is $\varphi = 30^\circ$. The simulation is conducted over 15 loading increments.

~~3D simulation results: snapshots of total pressure. Panel (a) shows the 3D view of total pressure. Panel (b) shows the YZ-slice of the full 3D model.~~

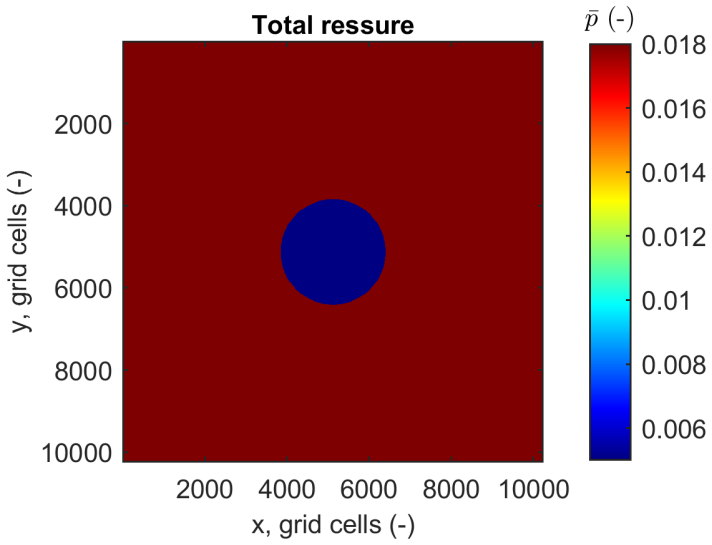

Figure 7. Geometry of the 2D simulation domain: a circular pressure anomaly is located at the center of the model. The resolution is $N = 10,239^2$ grid cells.

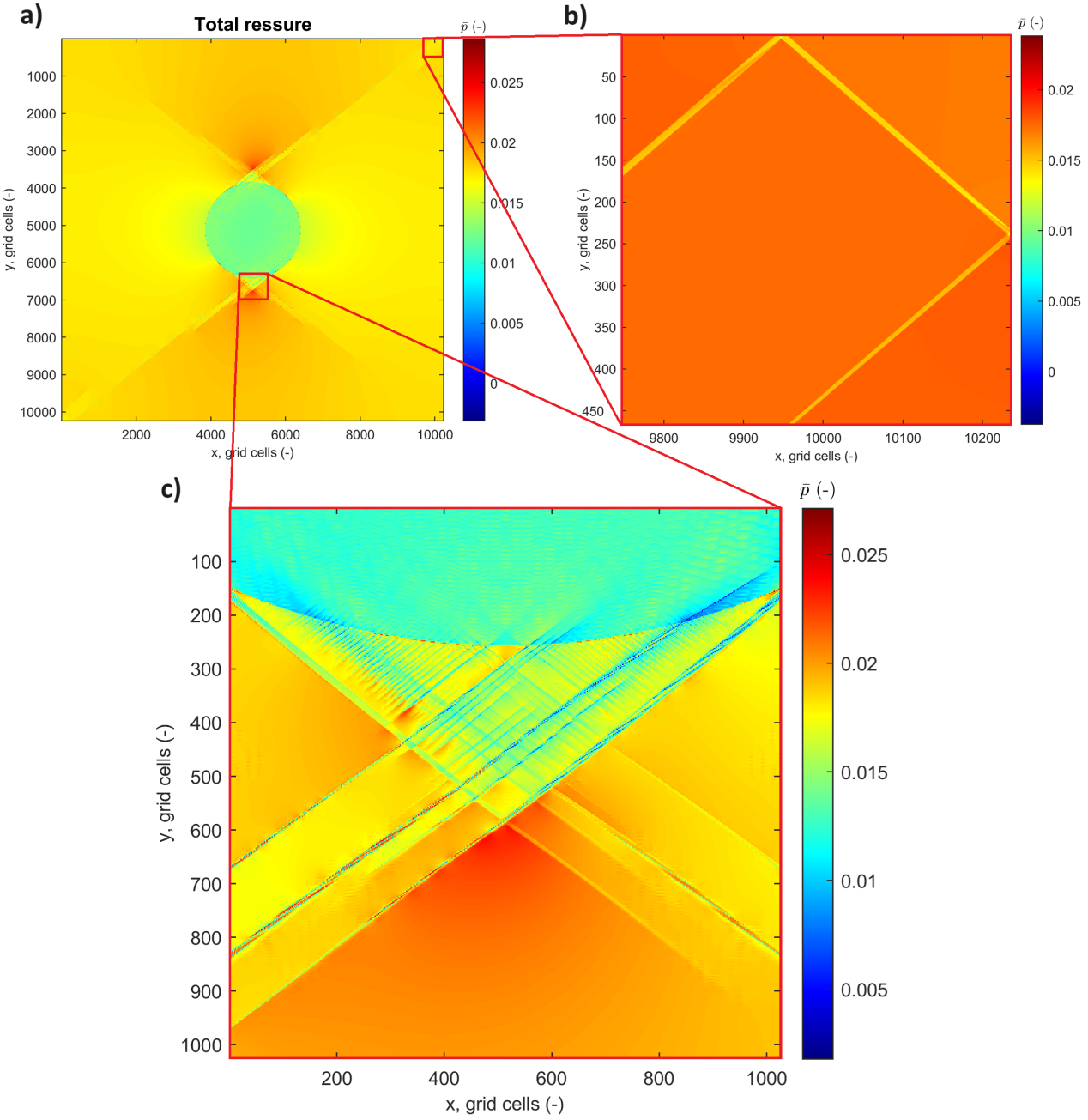

Figure 8. 2D simulation results: snapshots of total pressure. Panel (a) shows the full model, while panels (b) and (c) present zoomed-in views of the full model. The resolution is $N = 10,239^2$ grid cells.

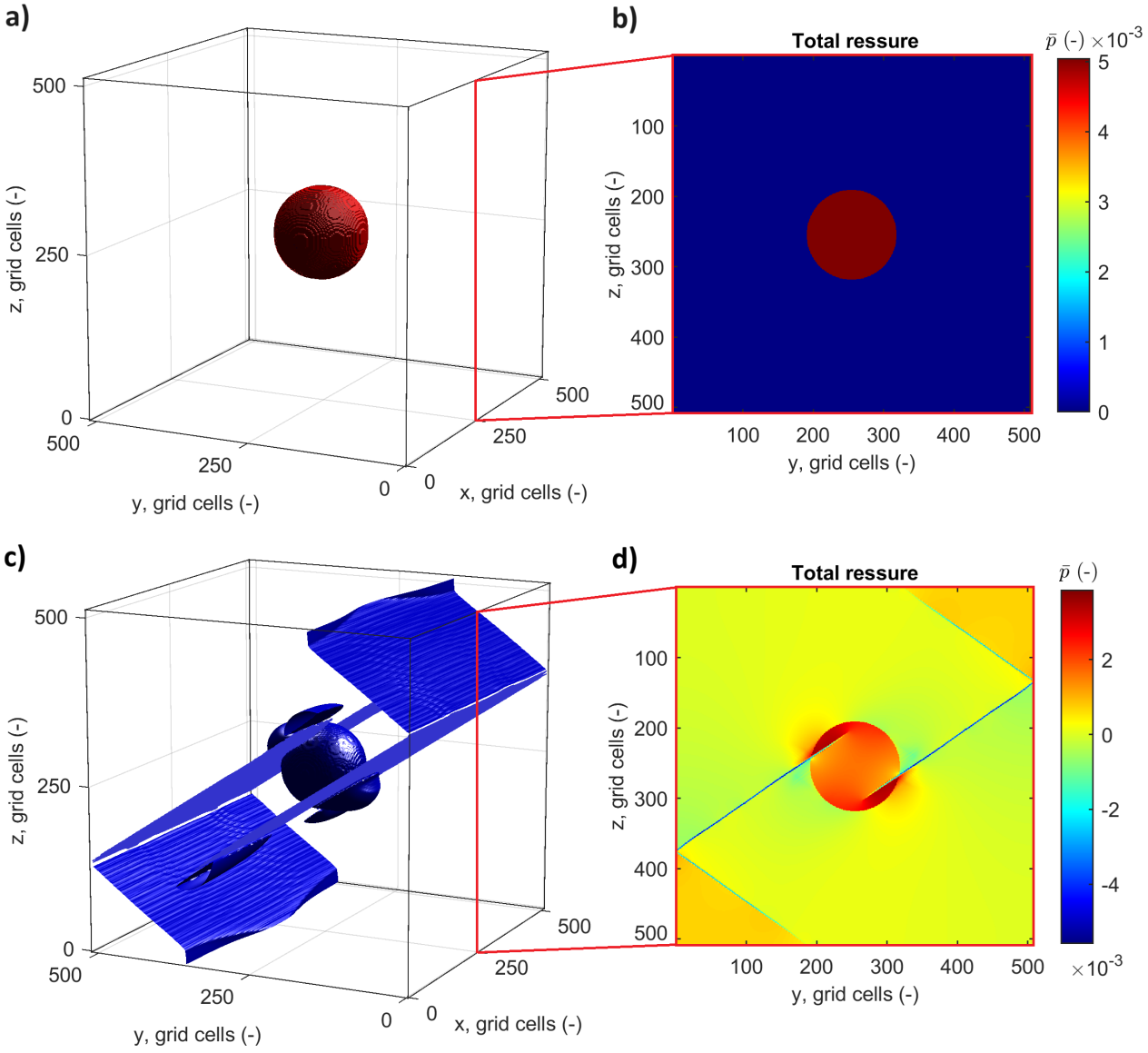

Figure 9. Geometry of the 3D simulation domain: a spherical pressure anomaly is located at the center. Panel (a) corresponds to 3D view, panel (b) corresponds to a slice in YZ-plane). Lower panels: 3D simulation results; snapshots of total pressure. Panel (c) shows the 3D view of total pressure. Panel (d) shows the YZ-slice of the full 3D model. The resolution is $N = 512^3$ grid cells.

6 Discussion

In this section, we analyze the implications of the numerical results presented in the previous sections and establish connections with relevant works in the field. We explore the behavior of the numerical parameters, such as the Strouhal number (St), and their optimal values for different physical models including elastic, viscoelastic, and poroelastic media. Additionally, we assess the influence of dimensionality, initial and boundary conditions, and non-linearities such as plasticity on the convergence and accuracy of the simulations. This analysis serves as a foundation for further extending these methods to more complex and realistic scenarios.

6.1 Incompressible equations: a connection with the work by Räss et al. (2022)

Räss et al. (2022) performed a comprehensive analysis of the APT method for various problems. However, the work by Räss et al. (2022) was restricted mainly to single-phase media and to incompressible equations. We here provide connections of the present work to the analysis presented by Räss et al. (2022).

In the present paper we deal with compressible elastic, viscoelastic or poroelastic equations. As a result, the only numerical parameter that has to be identified is the Strouhal number, St, which is expressed as

$$\mathrm{St} = \frac{f L_x}{\widetilde{V}_p} = \frac{L_x}{\widetilde{V}_p \Delta t}, \tag{66}$$

where f is the frequency. However, in the incompressible scenario ($K \to +\infty$), an additional numerical parameter shows up: $r = \widetilde{K}/\widetilde{G}$ (which is the compressible case is defined as $r = \widetilde{K}/\widetilde{G} \equiv K/G$). Räss et al. (2022) discovered that for some specfic tasks, the value of r should also be explored as well as the optimal value of St (or, equivalently, Re in their notation). As a result, Räss et al. (2022) reported the optimal values of pairs — r and Re for each set of equations. A connection between the "numerical" Reynolds number Re (Räss et al., 2022) and the Strouhal number St is provided below.

For the incompressible viscous Stokes equation, Räss et al. (2022) defines the "numerical" Reynolds number, Re, as

$$\mathrm{Re} = \frac{\widetilde{\rho} V_p^{\mathrm{S}} L_x}{\mu_s}, \tag{67}$$

where V_p^{S} is the characteristic velocity scale for the incompressible Stokes equations

$$V_p^{\mathrm{S}} = \sqrt{\frac{\widetilde{K} + 2\widetilde{G}}{\widetilde{\rho}}}. \tag{68}$$

and μ_s is the shear viscosity. Quantities $\widetilde{K}$, $\widetilde{G}$ and $\widetilde{\rho}$ are the numerical parameters. Note that in the case of incompressible viscoelastic Stokes equations, the quantity μ_s is replaced by μ^{ve}:

$$\mu^{\mathrm{ve}} = \left(\frac{1}{G \Delta t} + \frac{1}{\mu_s} \right)^{-1}. \tag{69}$$

As a result, for the incompressible viscoelastic Stokes equations, the "numerical" Reynolds number, Re, is defined as

$$\mathrm{Re} = \frac{\widetilde{\rho} V_p^{\mathrm{S}} L_x}{\mu^{\mathrm{ve}}}, \tag{70}$$

In the present paper, from the equation (27) for viscoelastic media, we can infer the Strouhal number:

$$\mathrm{St} = \frac{\widetilde{\rho}\widetilde{V}_p L_x}{\widetilde{H}^{\mathrm{ve}}}. \tag{71}$$

~~and $\widetilde{H}^{ve}$ is defined as~~

$$\underline{H^{\mathrm{ve}} = \left(\frac{1}{H\Delta t} + \frac{1}{\mu_s}\right).}$$

Note, that the full similarity between the definitions of Re (equation (70)) and Strouhal number (equation (71)). Indeed, $\mu^{\mathrm{ve}} \equiv H^{\mathrm{ve}}$ if we neglect the physical bulk modulus K (we keep only the shear modulus G), V_p^{S} is the characteristic "numerical" velocity which has the same meaning as $\widetilde{V}_p$ for a specific problem. Therefore, all the results presented by Räss et al. (2022) for incompressible equations can be extrapolated for compressible ones by using the results of the present paper.

6.2 Two- and three-dimensional simulations

As can be seen form the present study, the optimal values are similar for elastic, viscoelastic and poroelastic problems but depend on some physical input parameters. We here report the optimal values for St considering elasticity equations. The results can also be applied to viscoelastic and poroelastic problems by modifying the expressions for $\mathrm{St}_{\mathrm{opt}}$.

Numerical tests considering elasticity equations show that the provided values for $\mathrm{St}_{\mathrm{opt}}$ remain valid in 1D, 2D, and 3D. However, in 2D,

$$\mathrm{St} = \mathrm{St}_{\mathrm{opt}}^{\mathrm{2D}} \approx 2\pi\sqrt{2}, \tag{72}$$

and, in 3D,

$$\mathrm{St} = \mathrm{St}_{\mathrm{opt}}^{\mathrm{3D}} \approx 2\pi\sqrt{3}. \tag{73}$$

Note that in 3D, the value of $\mathrm{St}_{\mathrm{opt}}^{\mathrm{3D}}$ can be higher and depends on the initial and boundary conditions, the medium's heterogeneities, and the physics involved. A typical number of iterations over the pseudo-time depends on the problem size (in grid cells), the convergence rate and the desired precision. Form our experiments, a typical 3D heterogeneous model requires from $5 \times n_x$ to $20 \times n_x$ (n_x is the number of grid cells in x-dimension) iterations over the pseudo-time to achieve the quasi-static solution.

6.3 ~~The~~ Influence of ~~Boundary Conditions~~boundary conditions in 3D: elastic and elasto-plastic models

~~Figure ?? presents 2D and~~ Let us consider a 3D numerical domain with $L_x = L_y = L_z = 1$. Figure 10 presents 3D numerical results for the ~~elasto-plastic medium(for the formulation, see Alkhimenkov et al. (2024b))~~elastic medium. The numerical outcomes are analyzed as a function of ~~the stability parameter~~ St.

~~In the 2D simulation (Figure ??a), the~~ The total number of iterations over the pseudo-time is ~~3000~~1000, with a grid resolution of ~~$N = 511^2$~~ $N = 127^3$ cells. The results indicate that the optimal value of St is ~~$\mathrm{St} = 2\pi\sqrt{2}$~~close to $\mathrm{St} = 2\pi\sqrt{3}$, which is

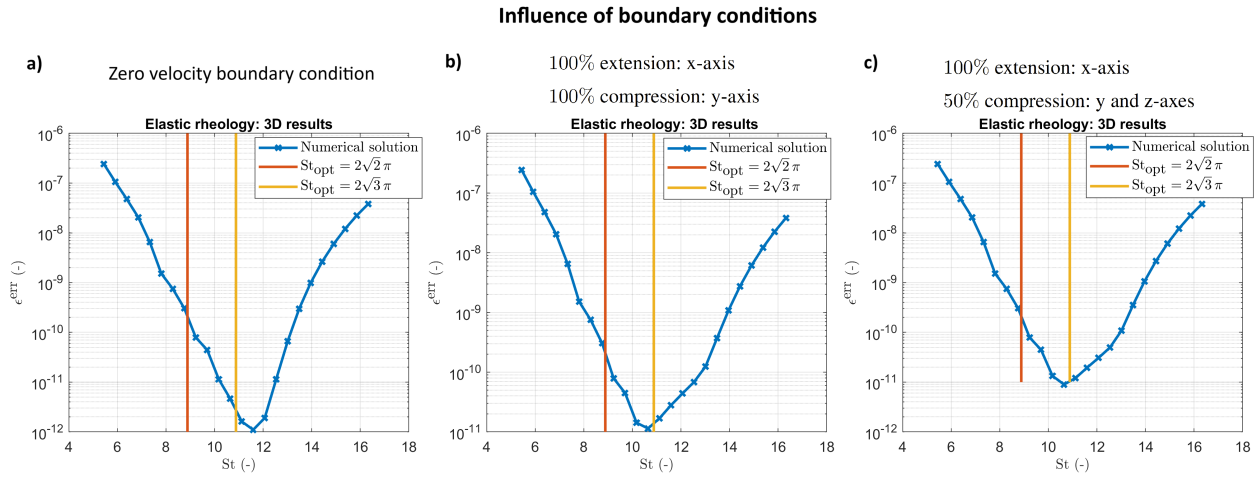

Figure 10. Numerical results in 3D (panels a, b and c): convergence in an elastic medium as a function of St. The parameter ϵ^{err} corresponds to the error magnitude of the APT scheme. Simulations in panels (a), (b) and (c) are identical except for the different boundary conditions.

typically valid for homogeneous media and appears to be ~~approximately~~ valid here as well, despite ~~the slight heterogeneity of the~~ different boundary conditions applied.

Figure 11 presents 3D numerical results for the elasto-plastic medium ~~.~~ (for a detailed formulation, see Alkhimenkov et al. (2024b)). The numerical outcomes are analyzed as a function of St. These simulations correspond to the loading scale where plastic flow is activated. The results indicate that the optimal value of St is similar to $St = 2\pi\sqrt{3}$ in the simulations where plasticity is not activated (i.e., purely elastic). This suggests that the presence of plasticity, which introduces significant non-linearity, does not notably affect the choice of optimal convergence parameters in this specific ~~2D~~ 3D case.

~~In the~~

6.4 Influence of initial conditions in 3D: elastic model

We consider a 3D ~~simulations (Figures ??b-c), the~~ numerical domain with $L_x = L_y = L_z = 1$. Figure 12 presents 3D numerical results for the elastic medium. Different panels correspond the the identical simulations but with different initial conditions. The numerical outcomes are analyzed as a function of St. The total number of iterations over the pseudo-time is ~~1500~~1000, with a grid resolution of ~~$N = 191^3$ cells. For the simulation depicted in Figure ??b, pure shear boundary conditions are applied along the x- and y-axes. In contrast, the simulation in Figure ??c uses the same model parameters but with slightly modified boundary conditions: 100% extension along the x-axis and 50% compression along the y- and z-axes. The results reveal~~ $N = 127^3$ cells. The results indicate that the optimal value of ~~St_{opt} is highly sensitive to the boundary conditions used. The optimal values of St_{opt} discussed in the previous section are accurate only for homogeneous media and specific initial and boundary conditions~~St is slightly different from $St = 2\pi\sqrt{3}$. We attribute it to different initial conditions applied which are the combinations of cos and sin functions across X, Y and Z-axes.

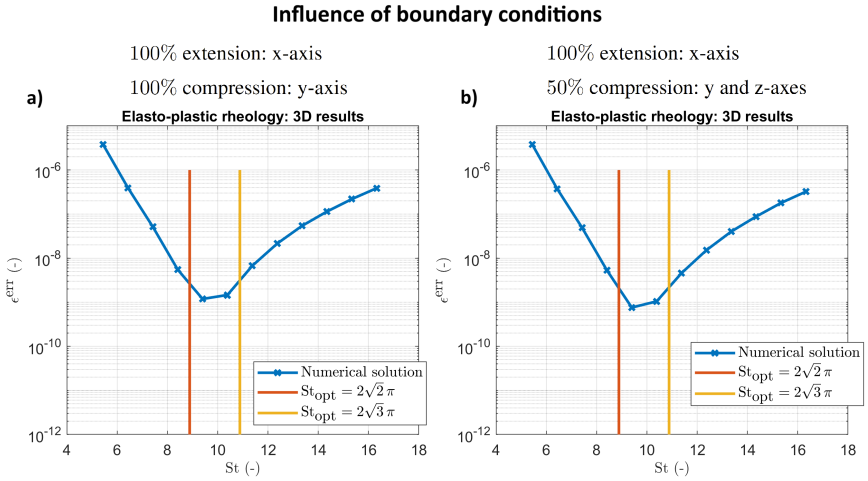

Figure 11. Numerical results in 3D (panels b and c): convergence in an elasto-plastic medium as a function of St. The parameter ϵ^{err} corresponds to the error magnitude of the APT scheme. Simulations in panels (a) and (b) are identical except for the different partitioning of pure shear boundary conditions.

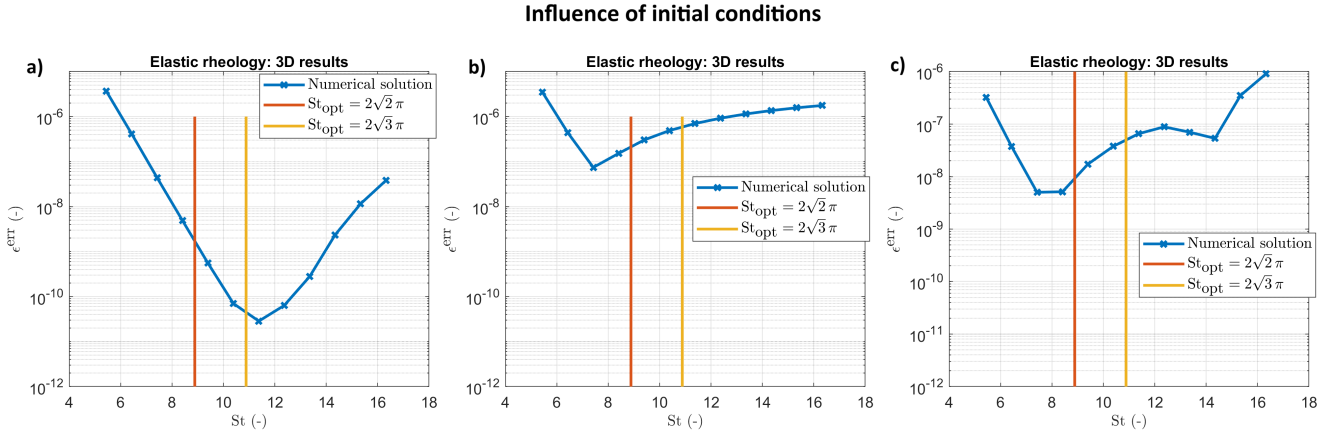

Figure 12. Numerical results in ~~2D (panel a) and~~ 3D (panels a, b and c): convergence in ~~a heterogeneous elasto-plastic~~ an elastic medium as a function of St. The parameter ϵ^{err} corresponds to the error magnitude of the APT scheme. Simulations in panels (a), (b) and (c) are identical except for the different ~~partitioning~~ initial conditions. Panel (a) corresponds to initial conditions of ~~pure shear boundary~~ cos function in X, Y and Z-axes. Panel (b) correspond to initial conditions of cos function in X, Y-axes and sin function in Z-axis. Panel (c) corresponds to initial conditions of sin function in X, Y and Z-axes.

6.5 General ~~Applicability~~applicability: ~~Influence~~ influence of ~~Initial~~ initial and ~~Boundary Conditions~~boundary conditions, ~~Non-linearities~~non-linearities, and ~~Coupling~~coupling

This study demonstrates that in homogeneous media with specific initial and boundary conditions, the optimal values of key numerical parameters, such as $\mathrm{St}_{\mathrm{opt}}$, can be accurately predicted across 1D, 2D, and 3D domains. This accuracy holds particularly true in the context of coupled systems of equations, as exemplified by the poroelastic models presented here. However, when dealing with more complex and realistic scenarios, special considerations are required to maintain this accuracy.

Our numerical experiments highlight that factors such as initial ~~and boundary~~ conditions, medium heterogeneities, and the presence of coupling and non-linearities (e.g., plasticity) can ~~significantly~~ influence the optimal values of numerical parameters. For instance, while in homogeneous and idealized conditions, the choice of $\mathrm{St}_{\mathrm{opt}}$ may remain relatively stable, introducing ~~heterogeneities or non-linear behavior, such as plasticity, necessitates a~~ different initial condition, necessitates a slight reassessment of these parameters. The study of strain localization ~~in both 2D and~~ (i.e., elasto-plastic rheology) in 3D models has shown that the presence of plasticity, which introduces strong non-linearities, can ~~alter~~ slightly modify the convergence characteristics~~, although in some cases, the optimal parameters remain surprisingly robust.~~

~~Furthermore, the~~ . The sensitivity of $\mathrm{St}_{\mathrm{opt}}$ to boundary conditions was ~~particularly evident~~ only minor in the 3D simulations~~, where even minor adjustments to the boundary conditions led to changes in the optimal parameter values~~. This suggests that ~~while~~ our approach can provide a strong starting point for selecting numerical parameters~~, the specific conditions of each problem must be carefully considered~~. In practical applications, where media may be heterogeneous, and boundary and initial conditions complex, this study provides a framework for estimating St_{opt} ~~and other numerical parameters~~. However, to ensure the accuracy and efficiency of simulations, it is recommended to conduct additional test simulations. These tests are necessary to fine-tune the parameters based on the specific characteristics of the model~~, such as the degree of heterogeneity, the type of non-linearities involved, and the nature of the coupling between different physical processes~~.

7 Conclusions

In this study, we ~~conducted a rigorous~~ performed a comprehensive analysis of the Accelerated Pseudo-Transient (APT) method for solving elastic, viscoelastic, and coupled hydro-mechanical problems, ~~particularly~~ specifically those governed by quasi-static Biot's poroelastic equations ~~across~~ in 1D, 2D, and 3D domains. We identified ~~and reported~~ the optimal numerical parameters ~~required to achieve rapid convergence for~~ for rapid convergence in elastic, viscoelastic, and poroelastic ~~problems. By systematically exploring these parameters across different spatial dimensions, we provided valuable~~ simulations, offering insights into the ~~applicability and~~ efficiency of the APT method ~~for a wide range of physical models~~across various spatial dimensions.

Our ~~study highlighted the effectiveness of the APT method~~results demonstrated the method's effectiveness in handling complex coupled systems and ~~demonstrated its robustness across various types of media, including~~ its robustness in both homogeneous and heterogeneous ~~conditions~~media. By comparing ~~our numerical results against~~ numerical results with ana-

lytical solutions for elastic equations, we validated the accuracy and reliability of the APT method~~in both homogeneous and heterogeneous settings~~.

We ~~investigated the influence~~ explored the impact of initial and boundary conditions, non-linearities, and coupling on ~~the~~ optimal numerical parameters, emphasizing the importance of adaptability in real-world applications. ~~Our findings suggest that while~~ While the APT method ~~offers a robust~~ provides a strong framework for selecting numerical parameters, ~~additional~~ further refinement is often ~~necessary when dealing with heterogeneous media and complex boundary conditions. This adaptability is crucial for extending the applicability of the APT method to more realistic and challenging scenarios encountered in geomechanics and other fields involving coupled hydro-mechanical processes.~~ needed for practical applications.

To illustrate the ~~flexibility of the APT method~~APT method's flexibility, we addressed ~~the nonlinear mechanical problem of~~ strain localization in ~~both~~ 2D and 3D contexts using a poro-elasto-viscoplastic ~~rheological model. We employed extremely high resolutions -~~ model, employing high resolutions ($10,000^2$ ~~voxels~~ in 2D and 512^3 ~~voxels~~ in 3D~~- which, to the best of our knowledge, have not been explored before for poro-elasto-viscoplastic rheology~~), which has not been extensively explored before. This model~~is grounded in a hypoelastic-based constitutive frameworkthat accommodates the simulation of large strains.~~

~~Importantly, the results presented in this paper are fully reproducible. To facilitate further research and verification, ~~, based on a hypoelastic constitutive framework, accommodates large strain simulations. All results are reproducible, and we have made ~~available Matlab, symbolic~~ the Matlab, Maple scripts, and CUDA C codes publicly available in a permanent repository.

Code availability. The software developed and used in the scope of this study is licensed under MIT License. The latest versions of the code is available from a permanent DOI repository (Zenodo) at: https://doi.org/10.5281/zenodo.14056939 (last access: 08 November 2024) (Alkhimenkov and Podladchikov, 2024). The repository contains code examples and can be readily used to reproduce the figures of the paper. The codes are written using the Matlab, Maple and CUDA C programming languages. Refer to the repositories' README for additional information

Appendix A: First PT and APT methods

A0.1 The Richardson Method for elliptic equations

Let us write the the simplest version of the relaxation method to solve an elliptic equation of quasi-static elasticity:

$$\begin{cases} \sigma_{xx} = (K + \frac{4}{3}G)\dfrac{\partial u_x}{\partial x} \\ 0 = \dfrac{\partial \sigma_{xx}}{\partial x} - \mu \dfrac{\partial u_x}{\partial \widetilde{t}}, \end{cases} \tag{A1}$$

where u_x is the displacement, $\widetilde{t}$ is a "pseudo" time and μ is a damping parameter. The system of equations (A1) represents a diffusive-type physical behavior in pseudo-time. The system is solved once the term $\partial u_x/\partial \widetilde{t}$ converges to zero with a certain precision (e.g., 10^{-12}). The convergence of this type of equation is $\sim n_x^2$, where n_x is the number of grid cells in x-direction. Such convergence rate makes this method impractical for large 3D problems, therefore, this method is not analyzed here. An interested reader can find more details in Frankel (1950).

A0.2 The accelerated pseudo-transient method: initial damping scheme

Now, let us consider a more advanced version of the pseudo-transient which we will call the accelerated pseudo-transient method (APT):

$$\begin{cases} \sigma_{xx} = (K + \frac{4}{3}G)\dfrac{\partial u_x}{\partial x} \\ \widetilde{\rho}\dfrac{\partial v_x}{\partial \widetilde{t}} = \dfrac{\partial \sigma_{xx}}{\partial x} - \mu v_x \\ \dfrac{\partial u_x}{\partial t} = v_x \end{cases} \tag{A2}$$

where μ and $\widetilde{\rho}$ are the damping parameters, t is the physical time which is linked to a loading increment. The system (A2) is solved once the terms $\partial v_x/\partial \widetilde{t}$ and μv_x converge to zero with a certain precision (e.g., 10^{-12}). The advantage of this system of equations (A2) over (A1) is that now the system of equations (A2) describes propagating waves in pseudo physical space and pseudo-time (i.e., hyperbolic), and, therefore, the convergence rate is $\sim n_x$ (compared to $\sim n_x^2$ in the Richardson Method for elliptic equations (A1)). An interested reader is refereed to Poliakov et al. (1993b, a) for more details regarding this damping scheme.

Appendix B: Quasi-static elasticity equations

Let us decompose the stress tenor into pressure and deviatoric stress tensor:

$$\sigma_{xx} = -p + \tau_{xx}. \tag{B1}$$

Now, the system of equations (4) can be rewritten as

$$\begin{cases} \dfrac{\partial p}{\partial t} = -K \dfrac{\partial v_x}{\partial x} \\ \dfrac{\partial \tau_{xx}}{\partial t} = 2G \left(\dfrac{\partial v_x}{\partial x} - \dfrac{1}{3} \dfrac{\partial v_x}{\partial x} \right) \\ 0 = \dfrac{\partial (-p + \tau_{xx})}{\partial x}. \end{cases} \tag{B2}$$

The quasi-static elasticity equations (B2) can then be re-written with the pseudo-time $\widetilde{t}$,

$$\begin{cases} \dfrac{1}{\widetilde{K}} \dfrac{\partial p}{\partial \widetilde{t}} + \dfrac{1}{K} \dfrac{p - \hat{p}}{\Delta t} = -\dfrac{\partial v_x}{\partial x} \\ \dfrac{1}{2\widetilde{G}} \dfrac{\partial \tau_{xx}}{\partial \widetilde{t}} + \dfrac{1}{2G} \dfrac{\tau_{xx} - \hat{\tau}_{xx}}{\Delta t} = \left(\dfrac{\partial v_x}{\partial x} - \dfrac{1}{3} \dfrac{\partial v_x}{\partial x} \right) \\ \widetilde{\rho} \dfrac{\partial v_x}{\partial \widetilde{t}} = -\dfrac{\partial \sigma_{xx}}{\partial x}, \end{cases} \tag{B3}$$

where $\hat{p}$ is the pressure field at the previous physical time step and and $\hat{\tau}_{xx}$ in the deviatoric stress at the previous physical time step.

The system of equations (B3) can be simplified:

$$\begin{cases} \dfrac{1}{\widetilde{K}} \dfrac{\partial p}{\partial \widetilde{t}} + \dfrac{1}{K} \dfrac{p}{\Delta t} = -\dfrac{\partial v_x}{\partial x} \\ \dfrac{1}{2\widetilde{G}} \dfrac{\partial \tau_{xx}}{\partial \widetilde{t}} + \dfrac{1}{2G} \dfrac{\tau_{xx}}{\Delta t} = \left(\dfrac{\partial v_x}{\partial x} - \dfrac{1}{3} \dfrac{\partial v_x}{\partial x} \right) \\ \widetilde{\rho} \dfrac{\partial v_x}{\partial \widetilde{t}} = -\dfrac{\partial (-p + \tau_{xx})}{\partial x}. \end{cases} \tag{B4}$$

$\widetilde{H} = \widetilde{K} + \frac{4}{3}\widetilde{G} = K + \frac{4}{3}G$, $\widetilde{K} = K$ and $\widetilde{G} = G$. The optimal value of St is the same as for the system (5) (or (6)):

$$\mathrm{St} = \mathrm{St}_{\text{opt}} = 2\,\pi, \tag{B5}$$

which corresponds to the fastest attenuation of propagating waves. The stress tenor in decomposed into pressure and deviatoric stress tensor, therefore, the following expressions are also provided

$$\widetilde{G}\Delta\widetilde{t} = (\widetilde{V}_p\,\Delta\widetilde{t})^2 \left(\frac{\Delta\widetilde{t}}{\widetilde{\rho}}\right)^{-1} \left(K_G + \frac{4}{3}\right)^{-1}, \tag{B6}$$

where $K_G = K/G$, and

$$\widetilde{K}\Delta\widetilde{t} = K_G\,\widetilde{G}\Delta\widetilde{t}. \tag{B7}$$

Appendix C: Discretization: quasi-static elasticity equations

Let us write the discrete form of the system (6). We use a classical conservative staggered space-time grid discretization (Virieux, 1986) which is equivalent to a finite volume approach (Dormy and Tarantola, 1995). More details on the present discretization can be found in Alkhimenkov et al. (2021b, a). Let us consider a physical domain L_x that is discretized into grid cells such that $L_x = n_x\,\Delta x$. The physical time t is also discretized as Δt ($\Delta\widetilde{t}$ is the pseudo-time). The resulting discrete form of the system (6) is

$$\begin{cases} \dfrac{1}{\widetilde{H}}\dfrac{[\sigma_{xx}]_i^{l+1/2} - [\sigma_{xx}]_i^{l-1/2}}{\Delta\widetilde{t}} + \dfrac{1}{H}\dfrac{[\sigma_{xx}]_i^{l+1/2}}{\Delta t} = \dfrac{[v_x]_{i+1/2}^{l} - [v_x]_{i-1/2}^{l}}{\Delta x} \\ \widetilde{\rho}\dfrac{[v_x]_{i+1/2}^{l+1} - [v_x]_{i+1/2}^{l}}{\Delta\widetilde{t}} = \dfrac{[\sigma_{xx}]_{i+1}^{l+1/2} - [\sigma_{xx}]_i^{l+1/2}}{\Delta x}. \end{cases} \tag{C1}$$

The discrete form of the system (B3) can be written as

$$\begin{cases} \dfrac{1}{\widetilde{K}}\dfrac{p_i^{l+1/2} - p_i^{l-1/2}}{\Delta\widetilde{t}} + \dfrac{1}{K}\dfrac{p_i^{l+1/2} - \hat{p}_i^{l+1/2}}{\Delta t} = -\dfrac{[v_x]_{i+1/2}^{l} - [v_x]_{i-1/2}^{l}}{\Delta x} \\ \dfrac{1}{2\widetilde{G}}\dfrac{[\tau_{xx}]_i^{l+1/2} - [\tau_{xx}]_i^{l-1/2}}{\Delta\widetilde{t}} + \dfrac{1}{2G}\dfrac{[\tau_{xx}]_i^{l+1/2} - [\hat{\tau}_{xx}]_i^{l+1/2}}{\Delta t} = \ldots \\ \qquad\qquad = \left(\dfrac{[v_x]_{i+1/2}^{l} - [v_x]_{i-1/2}^{l}}{\Delta x} - \dfrac{1}{3}\dfrac{[v_x]_{i+1/2}^{l} - [v_x]_{i-1/2}^{l}}{\Delta x}\right) \\ \widetilde{\rho}\dfrac{[v_x]_{i+1/2}^{l+1} - [v_x]_{i+1/2}^{l}}{\Delta\widetilde{t}} = -\dfrac{(-(p_{i+1}^{l+1/2} - p_i^{l+1/2}) + [\tau_{xx}]_{i+1}^{l+1/2} - [\tau_{xx}]_i^{l+1/2})}{\Delta x}, \end{cases} \tag{C2}$$

Appendix D: Matlab code

Listing 1. MATLAB Code for time loop computations

```
clear, figure(1), clf
%physics
Lx     = 1;
w      = pi;
u0     = 1;
G0     = 1;
K0     = 1*G0;
%numerics
nx     = 401;
nt     = 1e6;
K_G    = 1;
G      = 1;
K      = 1*G;
CFL    = 1/1.001;
%preprocessing
dx     = Lx/(nx-1);
x      = 0:dx:Lx;
for ipar = 1:25
    par      = 1+ipar/3;
    St      = par;
    dt       = 1;
    Vpdt     = dx*CFL;
    H        =  (K0+4/3*G0).*dt;
    dt_rho   = Vpdt.*Lx./St./H;
    Hdt      = Vpdt^2./dt_rho/1;
    Hr       = Hdt./(H);
    % initial
    V        = u0*sin(w*x/Lx);
    sigma       = 1*diff(V);

    for it = 1:nt
        sigma        = (sigma + Hdt.*(diff(V)/dx   ))./(1 + Hr);
        V(2:end-1) = V(2:end-1)      + dt_rho*diff(sigma)/dx;
        if it == 1, mfun        = max(abs(V)) + max(abs(sigma));   end
        if (max(abs(V)) + max(abs(sigma))) < 1e-9*mfun,break;end
    end
    iters1(ipar) = it;    ipars1(ipar) = par;
    Maximum = iters1/nx; [find, find2] = min(Maximum(:)) ;
end
Reopt_num = ipars1(find2);
omega = 1; iparmax = 25;
for ipar = 1:iparmax
    par   = 1+ipar/3 ;
    St   = par;
    rho   = St^2*H^2/((1*K+4/3*G)*Lx^2);
    dt    = dx/sqrt((1*K+4/3*G)/rho);
    Vs    = sqrt((1*K+4/3*G)/rho); fun    = 1;
    for it = 1:nt
        fun_old=fun;
        a1 = pi^2*St*omega^2;
        a2= pi^2 + 1*St^2 ;
        a3= 2*St ;
        a4= 1;
        A = [a1 a2 a3 a4];
        Pol2        = roots( flip(A));        lambda       = max(real(Pol2));
        fun         = exp(  lambda(1)*Vs*it*dt ./Lx     ) ;
        if it == 1, mfun        = max(abs(   exp( lambda(1)*Vs*it*dt./Lx   )  ));   end
        err         = fun - fun_old;        merr        = max(abs(fun));
        if merr*6 < 1.0 *1e-9*mfun,break,end
    end
    iters(ipar)     = it;
end
figure(1);clf
plot(ipars1,iters1/nx,'-x','LineWidth',1 )
hold on; plot( 1+(1:iparmax)/3 ,iters/nx, 'o','MarkerSize',10,'LineWidth',1.5);  hold on;
Re_opt = 2*pi;
plot( [Re_opt Re_opt],[5 15],'LineWidth',3);hold on
plot( [Reopt_num Reopt_num],[5 15],'LineWidth',3); hold on
xlabel( '$ {\mathrm{St}}$ (-)','Interpreter','latex'  );
ylabel( '$ {n}_\textrm{iter}/n_x$ (-)','Interpreter','latex'  );
legend('Numerical solution','Analytical solution',...
    '$   {\mathrm{St}}_\textrm{opt} = 2  \pi $ ',...
    '${\mathrm{St}} - \textrm{numerical}$', 'Interpreter','latex');
grid on; drawnow
```

Appendix E: Discretization: viscoelasticity

The discrete form of the system (26) can be written as

$$\begin{cases} \dfrac{1}{\widetilde{K}}\dfrac{p_i^{l+1/2}-p_i^{l-1/2}}{\Delta\widetilde{t}}+\dfrac{1}{K}\dfrac{p_i^{l+1/2}}{\Delta t}=-\dfrac{[v_x]^l_{i+1/2}-[v_x]^l_{i-1/2}}{\Delta x} \\ \dfrac{1}{2\widetilde{G}}\dfrac{[\tau_{xx}]_i^{l+1/2}-[\tau_{xx}]_i^{l-1/2}}{\Delta\widetilde{t}}+\dfrac{1}{2G}\dfrac{[\tau_{xx}]_i^{l+1/2}-[\hat{\tau}_{xx}]_i^{l+1/2}}{\Delta t}+\dfrac{[\tau_{xx}]_i^{l+1/2}}{2\mu_s}=\ldots \\ \qquad\qquad =\left(\dfrac{[v_x]^l_{i+1/2}-[v_x]^l_{i-1/2}}{\Delta x}-\dfrac{1}{3}\dfrac{[v_x]^l_{i+1/2}-[v_x]^l_{i-1/2}}{\Delta x}\right) \\ \widetilde{\rho}\dfrac{[v_x]^{l+1}_{i+1/2}-[v_x]^l_{i+1/2}}{\Delta\widetilde{t}}=-\dfrac{(-(p_{i+1}^{l+1/2}-p_i^{l+1/2})+[\tau_{xx}]^{l+1/2}_{i+1}-[\tau_{xx}]_i^{l+1/2})}{\Delta x}. \end{cases} \tag{E1}$$

Appendix F: Discretization: quasi-static Biot's poroelastic equations

The discrete form of the system (41)-(43) can be written as

$$\begin{cases} \dfrac{1}{\widetilde{K}_1}\dfrac{[\bar{p}]_i^{l+1/2}-[\bar{p}]_i^{l-1/2}}{\Delta\widetilde{t}}+\dfrac{1}{K_u}\dfrac{[\bar{p}]_i^{l+1/2}-[\hat{\bar{p}}]_i^{l+1/2}}{\Delta t}=-\dfrac{[v_x]^l_{i+1/2}-[v_x]^l_{i-1/2}}{\Delta x}-B\dfrac{[q_x^D]^l_{i+1/2}-[q_x^D]^l_{i-1/2}}{\Delta x} \\ \dfrac{1}{\widetilde{K}_2}\dfrac{[p_f]_i^{l+1/2}-[p_f]_i^{l-1/2}}{\Delta\widetilde{t}}+\dfrac{1}{K_u}\dfrac{[p_f]_i^{l+1/2}-[\hat{p}_f]_i^{l+1/2}}{\Delta t}=-B\dfrac{[v_x]^l_{i+1/2}-[v_x]^l_{i-1/2}}{\Delta x}-\dfrac{B}{\alpha}\dfrac{[q_x^D]^l_{i+1/2}-[q_x^D]^l_{i-1/2}}{\Delta x} \end{cases}, \tag{F1}$$

$$\begin{cases} \dfrac{1}{2\widetilde{G}}\dfrac{[\overline{\tau}_{xx}]_i^{l+1/2}-[\overline{\tau}_{xx}]_i^{l-1/2}}{\Delta\widetilde{t}}+\dfrac{1}{2G_u}\dfrac{[\overline{\tau}_{xx}]_i^{l+1/2}}{\Delta t}=\left(\dfrac{[v_x]^l_{i+1/2}-[v_x]^l_{i-1/2}}{\Delta x}-\dfrac{1}{3}\dfrac{[v_x]^l_{i+1/2}-[v_x]^l_{i-1/2}}{\Delta x}\right) \end{cases}, \tag{F2}$$

$$\begin{cases} \widetilde{\rho}_t\dfrac{[v_x]^{l+1}_{i+1/2}-[v_x]^l_{i+1/2}}{\Delta\widetilde{t}}=-\dfrac{(-([\bar{p}]^{l+1/2}_{i+1}-[\bar{p}]_i^{l+1/2})+[\overline{\tau}_{xx}]^{l+1/2}_{i+1}-[\overline{\tau}_{xx}]_i^{l+1/2})}{\Delta x} \\ \widetilde{\rho}_a\dfrac{[q_x^D]^{l+1}_{i+1/2}-[q_x^D]^l_{i+1/2}}{\Delta\widetilde{t}}=-[q_x^D]^l_{i+1/2}-\dfrac{\frac{k}{\eta_f}([p_f]^{l+1/2}_{i+1}-[p_f]_i^{l+1/2})}{\Delta x} \end{cases}. \tag{F3}$$

Author contributions. YA designed the original study, developed codes and algorithms, performed benchmarks, created figures and edited the manuscript. YYP provided early work on accelerated PT methods, contributed to the original study design, developed codes and algorithms, helped out with the dispersion analysis, edited the manuscript, supervised the work.

Competing interests. The contact author has declared that none of the authors has any competing interests.

Acknowledgements. We thank Ivan Utkin and Lyudmila Khakimova for stimulating discussions.

Financial support. Yury Alkhimenkov gratefully acknowledges the support of the Swiss National Science Foundation (project number P500PN_206722).

References

Alkhimenkov, Y.: Numerical validation of Gassmann's equations, Geophysics, 88, A25–A29, 2023.

Alkhimenkov, Y. and Podladchikov, Y.: APTsolver, https://doi.org/10.5281/zenodo.14056939, 2024.

Alkhimenkov, Y., Khakimova, L., and Podladchikov, Y.: Stability of discrete schemes of Biot's poroelastic equations, Geophysical Journal International, 225, 354–377, 2021a.

Alkhimenkov, Y., Räss, L., Khakimova, L., Quintal, B., and Podladchikov, Y.: Resolving wave propagation in anisotropic poroelastic media using graphical processing units (GPUs), Journal of Geophysical Research: Solid Earth, 126, e2020JB021 175, 2021b.

Alkhimenkov, Y., Khakimova, L., and Podladchikov, Y.: Shear bands triggered by solitary porosity waves in deforming fluid-saturated porous media, Geophysical Research Letters, 51, e2024GL108 789, 2024a.

Alkhimenkov, Y., Khakimova, L., Utkin, I., and Podladchikov, Y.: Resolving Strain Localization in Frictional and Time-Dependent Plasticity: Two- and Three-Dimensional Numerical Modeling Study Using Graphical Processing Units (GPUs), Journal of Geophysical Research: Solid Earth, 129, e2023JB028 566, https://doi.org/https://doi.org/10.1029/2023JB028566, e2023JB028566 2023JB028566, 2024b.

Benyamin, M., Calder, J., Sundaramoorthi, G., and Yezzi, A.: Accelerated variational PDEs for efficient solution of regularized inversion problems, Journal of mathematical imaging and vision, 62, 10–36, 2020.

Biot, M. A.: Mechanics of deformation and acoustic propagation in porous media, Journal of applied physics, 33, 1482–1498, 1962.

Calder, J. and Yezzi, A.: PDE acceleration: a convergence rate analysis and applications to obstacle problems, Research in the Mathematical Sciences, 6, 35, 2019.

Cox, S. and Zuazua, E.: The rate at which energy decays in a damped string, Communications in partial differential equations, 19, 213–243, 1994.

Cundall, P.: Explicit finite-difference methods in geomechanics, Proc. 2nd Int. Cof. Num. Meth. Geomech., ASCE, New York, pp. 132–150, 1976.

Dormy, E. and Tarantola, A.: Numerical simulation of elastic wave propagation using a finite volume method, Journal of Geophysical Research: Solid Earth, 100, 2123–2133, 1995.

Duretz, T., de Borst, R., and Le Pourhiet, L.: Finite thickness of shear bands in frictional viscoplasticity and implications for lithosphere dynamics, Geochemistry, Geophysics, Geosystems, 20, 5598–5616, 2019.

Frankel, S. P.: Convergence rates of iterative treatments of partial differential equations, Mathematics of Computation, 4, 65–75, 1950.

Gassmann, F.: Uber die elastizitat poroser medien, Vierteljahrsschrift der Naturforschenden Gesellschaft in Zurich, 96, 1–23, 1951.

Hirsch, C.: Numerical computation of internal and external flows, Volume 1: Fundamentals of numerical discretization, John Wiley and Sons, 9, 10, 1988.

Landau, L. D. and Lifshitz, E. M.: Course of Theoretical Physics Vol 7: Theory of Elasticity, Pergamon press, 1959.

Li, S. and Wang, G.: Introduction to micromechanics and nanomechanics, World Scientific Publishing Company, 2008.

Nemat-Nasser, S. and Hori, M.: Micromechanics: overall properties of heterogeneous materials, Elsevier, 2013.

Omlin, S., Malvoisin, B., and Podladchikov, Y. Y.: Pore fluid extraction by reactive solitary waves in 3-D, Geophysical Research Letters, 44, 9267–9275, 2017.

Otter, J.: Computations for prestressed concrete reactor pressure vessels using dynamic relaxation, Nuclear structural engineering, 1, 61–75, 1965.

Otter, J. R. H., Cassell, A. C., Hobbs, R. E., and POISSON: Dynamic relaxation, Proceedings of the Institution of Civil Engineers, 35, 633–656, 1966.

Poliakov, A., Cundall, P., Podladchikov, Y., and Lyakhovsky, V.: An explicit inertial method for the simulation of viscoelastic flow: an evaluation of elastic effects on diapiric flow in two-and three-layers models, in: Flow and Creep in the Solar System: observations, modeling and Theory, pp. 175–195, Springer, 1993a.

Poliakov, A., Podladchikov, Y., and Talbot, C.: Initiation of salt diapirs with frictional overburdens: numerical experiments, Tectonophysics, 228, 199–210, 1993b.

Poliakov, A., HERRMANN, H. J., PODLADCHIKOV, Y. Y., and ROUX, S.: Fractal plastic shear bands, Fractals, 2, 567–581, 1994.

Polyak, B. T.: Some methods of speeding up the convergence of iteration methods, Ussr computational mathematics and mathematical physics, 4, 1–17, 1964.

Räss, L., Duretz, T., and Podladchikov, Y.: Resolving hydromechanical coupling in two and three dimensions: spontaneous channelling of porous fluids owing to decompaction weakening, Geophysical Journal International, 218, 1591–1616, 2019.

Räss, L., Licul, A., Herman, F., Podladchikov, Y. Y., and Suckale, J.: Modelling thermomechanical ice deformation using an implicit pseudo-transient method (FastICE v1. 0) based on graphical processing units (GPUs), Geoscientific Model Development, 13, 955–976, 2020.

Räss, L., Utkin, I., Duretz, T., Omlin, S., and Podladchikov, Y. Y.: Assessing the robustness and scalability of the accelerated pseudo-transient method, Geoscientific Model Development, 15, 5757–5786, 2022.

Richardson, L. F.: IX. The approximate arithmetical solution by finite differences of physical problems involving differential equations, with an application to the stresses in a masonry dam, Philosophical Transactions of the Royal Society of London. Series A, containing papers of a mathematical or physical character, 210, 307–357, 1911.

Riley, J. D.: Iteration procedures for the Dirichlet difference problem, Mathematical Tables and Other Aids to Computation, 8, 125–131, 1954.

Virieux, J.: P-SV wave propagation in heterogeneous media: Velocity-stress finite-difference method, Geophysics, 51, 889–901, 1986.

Wang, L. H., Yarushina, V. M., Alkhimenkov, Y., and Podladchikov, Y.: Physics-inspired pseudo-transient method and its application in modelling focused fluid flow with geological complexity, Geophysical Journal International, 229, 1–20, 2022.

Young, D. M.: Second-degree iterative methods for the solution of large linear systems, Journal of Approximation Theory, 5, 137–148, 1972.